

Article

Chemical Composition of Aerosol over the Arctic Ocean from Summer ARctic EXpedition (AREX) 2011–2012 Cruises: Ions, Amines, Elemental Carbon, Organic Matter, Polycyclic Aromatic Hydrocarbons, n-Alkanes, Metals, and Rare Earth Elements

Luca Ferrero ^{1,*} , Giorgia Sangiorgi ^{1,2}, Maria Grazia Perrone ^{1,3}, Cristiana Rizzi ¹, Marco Cataldi ¹, Piotr Markuszewski ⁴, Paulina Pakszys ⁴, Przemysław Makuch ⁴ , Tomasz Petelski ⁴, Silvia Becagli ⁵, Rita Traversi ⁵, Ezio Bolzacchini ¹ and Tymon Zielinski ⁴

¹ GEMMA and POLARIS Research Centre, Department of Earth and Environmental Sciences, University of Milano-Bicocca, 20126 Milan, Italy; giorgixi@gmail.com (G.S.); mariagrazia.perrone@gmail.com (M.G.P.); c.rizzi8@campus.unimib.it (C.R.); m.cataldi@campus.unimib.it (M.C.); ezio.bolzacchini@unimib.it (E.B.)

² UL Italy, via Europa 28, 22060 Cabiato, Italy

³ TCR Tecora, Via delle Primule 16, 20815 Cogliate, Italy

⁴ Institute of Oceanology, Polish Academy of Sciences, 81-712 Sopot, Poland; pmarkusz@iopan.pl (P.M.); pakszys@iopan.gda.pl (P.P.); makuch@iopan.pl (P.M.); petelski@iopan.gda.pl (T.P.); tymon@iopan.pl (T.Z.)

⁵ Department of Chemistry, University of Florence, Via della Lastruccia 3, 50019 Sesto F. no, Florence, Italy; silvia.becagli@unifi.it (S.B.); rita.traversi@unifi.it (R.T.)

* Correspondence: luca.ferrero@unimib.it; Tel.: +39-02-6448-2814

Received: 30 November 2018; Accepted: 19 January 2019; Published: 29 January 2019



Abstract: During the summers of 2011 and 2012, two scientific cruises were carried out over the Arctic Ocean aiming at the determination of the aerosol chemical composition in this pristine environment. First, mass spectrometry was applied to study the concentration and gas/particle partitioning of polycyclic aromatic hydrocarbons (PAHs) and n-alkanes. Experimental and modelled data of phase partitioning were compared: results demonstrated an equilibrium between gas and particle phase for PAHs, while n-alkanes showed a particle-oriented partitioning, due to the local marine origin of them, confirmed by the extremely low value of their carbon preference index. Moreover, the inorganic and organic ions (carboxylic acids and amines) concentrations, together with those of elemental carbon (EC) and organic matter (OM), were analyzed: 63% of aerosol was composed of ionic compounds (>90% from sea-salt) and the OM content was very high (30.5%; close to 29.0% of Cl⁻) in agreement with n-alkanes' marine signature. Furthermore, the amines' (dimethylamine, trimethylamine, diethylamine) concentrations were 3.98 ± 1.21 , 1.70 ± 0.82 , and 1.06 ± 0.56 p.p.t.v., respectively, fully in keeping with concentration values used in the CLOUD (Cosmics Leaving OUtdoor Droplet)-chamber experiments to simulate the ambient nucleation rate in a H₂SO₄-DMA-H₂O system, showing the amines' importance in polar regions to promote new particle formation. Finally, high resolution mass spectrometry was applied to determine trace elements, including Rare Earth Elements (REEs), highlighting the dominant natural versus anthropic inputs for trace metals (e.g., Fe, Mn, Ti vs. As, Cd, Ni) and possible signatures of such anthropic activity.

Keywords: aerosol; Arctic Ocean; inorganic ions; carboxylic acids; amines; elemental carbon; organic carbon; polycyclic aromatic hydrocarbon; n-alkanes; elements; Svalbard

1. Introduction

The Arctic is affected by global warming and the observed temperature increase is double compared with the rest of the globe [1–3]. This is the result of complex global feedbacks acting at different spatial and temporal scales that depend on aerosol's direct and indirect effects on the climate [1,4–8].

Shindell and Faluvegi [3] estimated that the globally decreasing concentrations of sulfate aerosols and the increasing concentrations of black carbon (due to its capability to heat the atmosphere [4–13]) contributed 1.09 ± 0.81 °C to the Arctic surface temperature increase of 1.48 ± 0.28 °C during 1976–2007. This phenomenology, was recently confirmed by Navarro et al. [9], which demonstrated that, starting from the 1980s, the declining European sulfur emissions affected the Arctic region with an additional 0.3 Wm^{-2} of energy and 0.5 °C on average annually; a situation that is amplified mainly in fall and winter. This is in agreement with the experimental results reported by Maturilli et al. [10] that showed an annual mean Arctic temperature rise of $+1.3 \pm 0.7$ K per decade, with a maximum seasonal increase during the winter months of $+3.1 \pm 2.6$ K per decade, while during summer the observed increase was up to 0.8 K per decade. Interestingly, Isaksen et al. [11] recently reported that the land-based surface air temperature and local and regional sea ice cover were affected by air masses from the east and north of Spitsbergen, which suggests that a major part of the atmospheric warming observed in Spitsbergen is driven by heat exchange from the larger open water area in the Barents Sea and the region north of Spitsbergen.

As the aerosol particles are short-living climate forcers (≈ 1 – 2 weeks of residence time) [12–15], their contribution to the Arctic amplification can be considered due to an interplay of the heat generated by aerosol at mid-latitudes (and transported to the Arctic) and the effects of the aerosol itself within the Arctic. The aerosol effects within the Arctic area can be due to the transport of aerosol pollution from source regions and to local emissions (e.g., ship emissions and gas flaring). These processes are well described by Sand et al. [16], in Serreze and Barry [17], and in Stohl et al. [18].

The results reported by Sand et al. [16] demonstrated that “black carbon (BC) alone can cause a warming in the Arctic by 0.5 degrees, but when also including all other short living climate forcers (SLCF), the net effect is a cooling of 0.44 degrees.” This is also in agreement with the phenomenology reported in Shindell and Faluvegi [3] when they discuss the regional climate response to forcing applied in various latitude bands: when BC acts within the Arctic itself (considering all the possible effects and feedbacks) can promote a negative cooling effect. A similar result is reported in Sand et al. [19] and is due to a combination of a weakening of the northward heat transport caused by a reduction in the meridional temperature gradient and a dimming at the surface. Moreover, aerosol particles can affect the sea ice extension both changing the heat fluxes between the ocean and the atmosphere [20,21] and influencing the secondary aerosol formation from the open sea itself [22]. Secondary aerosol can promote a further feedback affecting the cloud cover and thus the long-wave radiation fluxes [23].

Therefore, the aerosol properties within the Arctic area are fundamental to describe its role in climate modifications. The aerosol properties that are important for the climatic effect (e.g., optical, hygroscopic) are connected to the aerosol chemistry [24–26] and they change with time [27,28]. Thus, the time related chemical composition and the relative importance of long-range advection with respect to local emissions should be continuously monitored, and accounted for, in a pristine environment [3,19,29].

The aerosol chemical composition seasonally varies in the Arctic due to changes both in sources (outside or inside the Arctic region) and in meteorological conditions that may allow or inhibit the transport/local formation from source regions [15,30]. According to Stohl et al. [31], the late winter/springtime period is affected by the Arctic haze: an inflow of air pollution dominated by accumulation mode aerosol that can be transported into the Arctic both at low-level, or with an uplift outside the Arctic. In the former case, the transport is followed by ascent in the Arctic, while in the latter it is followed by descent in the Arctic itself. During summer, the high continental pressure disappears and the transport from medium latitudes becomes less relevant. However, new particle

formation (NPF) events, that start in early spring in the near-surface layer [32], are mostly manifested in summer [22,33] making the summer period dominated by small and fresh Aitken particles that are locally formed [22,34,35]. Moreover, during summer, NPF can be mixed and affected/changed by some emissions related to forest fires/biomass burning [36,37] and to local anthropogenic sources: the increasing of shipping emissions in the Arctic is a good example, as they inject BC and sulfate precursors directly into the Arctic [30,32,38].

All the aforementioned processes influence aerosol chemical composition (as well as the size). Thus, there is the need to measure aerosol properties, and especially various chemical markers (related to aerosol direct/indirect impact on climate) in the Arctic environment.

The dominant aerosol chemical markers (concentration-wise) over the Arctic Ocean are related to primary marine emissions. Particularly, chloride and sodium, as well magnesium and calcium (to some extent) are taken as reference parameters to quantify sea spray inputs. However, other chemical compounds present at lower concentrations, can be very important. In this respect, aliphatic amines are fundamental in promoting NPF [39,40]. In addition, n-alkanes (ALKs) can also be used to indicate the origin of aerosol organic matter (OM) from the sea. Particularly, as reported in Marty and Salot [41], the carbon preference index (CPI) is a useful parameter, which is calculated as a ratio of the sum of concentrations of the odd versus the even-numbered carbon ALKs. Over the sea, CPI can reach values close to 1 or lower as ALKs do not show a characteristic input from phytoplankton sources [42].

Carboxylic acids are among other important chemical markers, related to secondary organic aerosol (SOA) formation [43] and hygroscopic properties [26,44]. The major source for low molecular weight carboxylic acids is the photochemical oxidation of organic precursors in the atmosphere [45,46], but they can also be directly emitted via fossil fuel combustion [47] and biomass burning [48,49]. These compounds were reported in the Arctic and Antarctic atmospheric aerosols by the studies from Kawamura and Narukawa [45,50–53], who found that oxalic acid was the most abundant diacid species, followed by malonic, succinic, and glutaric acid.

Therefore, the knowledge of the organic material appears to be fundamental to reveal the aerosol impact on climate. In this respect, a growing attention is related to the brown carbon as it may contribute $\approx 10\text{--}30\%$ to the total aerosol absorption on a global scale [54,55]. Ferrero et al. [56] experimentally measured that the brown carbon accounts for $12.5 \pm 0.6\%$ of the total absorption, and due to fact that is present in biomass burning aerosol, it makes the biomass particles 1.63 ± 0.03 times more efficient than pure BC in heating the atmosphere. This means that any molecular component of brown carbon is worthy of attention. Laskin et al. [57] highlighted the role of PAHs in the brown carbon, especially when they undergo oxidation/nitration. At the same time, they are an important class of persistent organic pollutants (POPs) than can interact with the local ecosystem. Deposition trends of PAHs have shown a dramatic increase in concentrations over the last 100 years that correlate well with the historical record of world petroleum production [58]; however, a decreasing of their concentration was observed during the last decade [59]. A topic of great importance while studying PAHs, arises from their semi-volatility. The phase partitioning is an extremely important parameter because it affects their atmospheric fate, driving the permanence time in air, transport, and transformation [60–62]. Summertime conditions may enhance re-evaporation [63], favoring transport towards the Arctic with effects both on the climate and ecosystem. Up to now, most of the studies concerning the PAH gas-particle partitioning have been focused on urban areas [61,62,64–66], fewer addressed their behavior in rural/remote sites [67–70]. Thus, their partitioning is especially important in the Arctic, one of the coldest and most remote locations of the planet.

Other chemical components can be very important in the Arctic too, such as trace elements, including rare earth elements (REEs). Despite their low concentrations (with respect to other markers), they can provide relevant information about the source areas of the studied atmospheric aerosols thanks to their conservative character [71–73]. In fact, they usually keep the same original composition during the transport from the source area to the sampling site, even when they are transported for thousands of kilometers [74]. Thus, selected elements and their ratios can be taken as specific tracers

of natural and anthropic sources. REEs are particularly suitable for this purpose. Given the analytical limitations in their measurements (very low concentrations), trace elements and REEs data available from remote sites are limited to short or low temporal resolution sampling campaigns [75] or to a few continuous campaigns in the High Canadian Arctic [76] or Svalbard Islands [77]. Hence, the data set here presented from the Arctic Ocean offer a chance to enlarge the currently available information of these chemical tracers in polar areas.

In order to monitor all the mentioned chemical markers in the Arctic, some important measuring sites are present, for example Ny-Ålesund, which is a fully equipped site in which several monitoring stations (e.g., Zeppelin is one of the most important ones) are present (more than 15 nations work there). However, even though it is particularly suitable for aerosol studies due to the long-term data series available (aerosol properties, lidar profiles, radiometric and meteorological data) [22,30,32,34,35,78,79], in summer this land-based site can be influenced by ship emissions [32], thus reducing the capability to observe pure summertime aerosol properties in the Arctic pristine environment. Moreover, local micrometeorology can play a serious role influencing the land-based measurements [32,80].

Thus, this paper tries to fill this gap by reporting new data of aerosol chemical composition and molecular markers measured along two years of summertime cruises (2011 and 2012) on board of the Oceania research vessel (Institute of Oceanology Polish Academy of Sciences). An important feature of this vessel is the presence of three sailing masts, which enable the ship to reduce the engine use and thus any impact on aerosol sampling and chemistry determination. This allows for overcoming the limitation of land-based measuring stations, making it possible to measure the summertime aerosol properties on a wide area of the Arctic Ocean. Moreover this work provides: (1) the first comprehensive assessment of PAH gas and aerosol phase concentrations in the Arctic Ocean and a comparison with a gas/particle partitioning model; (2) a first important dataset of aliphatic amines; (3) an investigation of ALKs CPI to assess the marine origin of organic material; (4) the first assessment of atmospheric levels of major trace, minor trace, and rare earth elements in the Arctic Ocean; and (5) a comparison of the full bulk aerosol chemistry with modelling results. Finally, the obtained aerosol chemical composition was compared with that simultaneously measured at Ny-Ålesund.

We describe first the sampling platform (the ship) and the aerosol measurements in Section 2. Results and discussion follow in Section 3, with the conclusions in the final Section 4.

2. Experiments

2.1. Sampling Campaigns

Two sampling campaigns were performed in the summers of 2011 and 2012 (20 June to 12 August) on board the Oceania oceanographic ship (Institute of Oceanology Polish Academy of Sciences), within the framework of the Arctic Expedition (AREX).

Oceania has three sailing masts that enable the ship to reduce the engine use and thus any impact on aerosol sampling and chemistry determination (Figure 1). The campaigns started in Tromsø (Norway) and finished in the Svalbard Islands (Norway), performing a two-months long cruise during each summer along the Arctic Ocean; longitudinal and latitudinal transects encompassed the Norwegian and Greenland Seas (basically, the same route was followed during both the two campaigns; Figure 2).



Figure 1. Research vessel Oceania (left) and location of the total suspended particulate (TSP) sampler on the balcony (right) of the Oceania.

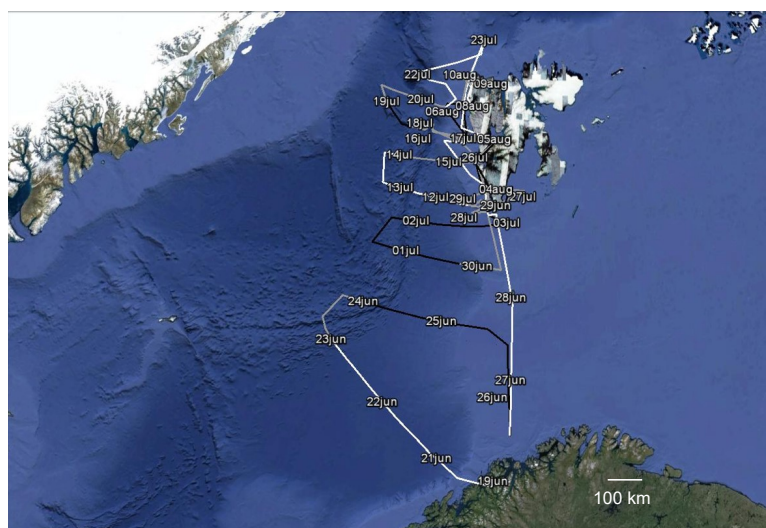


Figure 2. Route of the Oceania during the AREX cruises from Tromsø to Svalbard.

Total suspended particles (TSP) were collected for a total of 24 (summer 2011) and 14 (summer 2012) samples. Air samples were taken by using a high-volume sampler (ECHO-PUF, TCR Tecora, Milan, Italy) designed to simultaneously collect the particulate and gaseous phases of the air. The collection of the TSP was performed on quartz fiber filters (QFFs, diameter 105 mm; Whatman, Springfield Mill, UK). The gaseous compounds were captured only during 2011 by using a polyurethane foam cartridge (PUF, diameter 60 mm, length 76 mm, ORBOTM 2000; Supelco, Sigma-Aldrich, St. Louis, MO, USA). The air sampler was installed at 6 m above the upper deck of the ship (10 m above the sea level) and close to the bow (Figure 1). The high-volume sampler operated at 200 L min^{-1} , with an average sampling time of 48 h (summer 2011; average sampling volume = 566 m^3) and 72 h (summer 2012; average sampling volume = 805 m^3). The selected sampling flow rate minimized the sampling artifacts (sorption of gases on the filter and the volatilization of particle-bound compounds from the filter) [81]. Prior to sampling, the QFFs were baked at $600 \text{ }^\circ\text{C}$ for 2 h to reduce impurities and were then stored at room temperature wrapped in pre-cleaned (with ultrapure water, acetone, and hexane) aluminum foils. After sampling, the samples were stored in aluminum foils at $-20 \text{ }^\circ\text{C}$ in the dark, until analysis. Before and after sampling, the filters were

equilibrated (48 h at 35% RH, room temperature) and weighted with a microbalance (1 μg precision, model M5P-000V001; Sartorius, Göttingen, Germany) in order to measure the collected mass of TSP. At the same time, blank field filters were collected (six during summer 2011 and three during summer 2012). Considering the mass measured on blank field filters, the TSP detection limits were 1.2 $\mu\text{g m}^{-3}$ and 1.0 $\mu\text{g m}^{-3}$ for the 2011 and 2012 sampling filters, respectively.

Moreover, during AREX 2011 (20/06–30/07), PM_{10} samples were collected using a Tecora SkyPost sampler (1 $\text{m}^3 \text{h}^{-1}$, polytetrafluoroethylene (PTFE) filters 47 mm, 12 h time resolution). Samples were weighted before and after sampling in order to obtain the mass of the collected atmospheric particulate matter. All filters were conditioned for at least 24 h prior to weighing at a relative humidity of 35% and temperature of 25 °C.

Finally, PM_{10} samples were also collected, at the same time of AREX 2011 and AREX 2012 cruises, at Ny-Ålesund (Grubebadet site, 78°55′03″ N 11°53′40″ E) by using two parallel Tecora SkyPost low-volume sampler (EN 12341; PM_{10} sampling head, flow 2.3 $\text{m}^3 \text{h}^{-1}$; PTFE and quartz fiber filters, $\text{Ø} = 47 \text{ mm}$). PM_{10} samples collected with the first sampler (24 h on Pall R2PJ047 Teflon filters) were analyzed to determine the inorganic and organic ions; PM_{10} samples collected with the second sampler (96 h on pre-fired quartz microfiber filters chm QF1 grade) were analyzed to determine organic and elemental carbon. The analytical methods applied on the Ny-Ålesund samples were described in detail in Ferrero et al. [32] and in Udisti et al. [35]; we refer to these publications, as Ny-Ålesund data were used here for a comparison with the aerosol chemical composition measured over the Arctic Ocean. Therefore, in the remainder of the paper, the sample extraction and analysis are only described for samples collected along the AREX 2011 and AREX 2012 cruises.

2.2. Sample Extraction and Analysis

TSP samples were divided into three different portions, each one dedicated to a different analysis: (1) gas chromatography coupled with mass spectrometry (GC-MS; $\approx 3000 \text{ mm}^2$), (2) ion chromatography (IC; $\approx 1700 \text{ mm}^2$), and (3) carbon analyzer (150 mm^2). Uniformity of aerosol on filters was validated in a previous work [82]. The portions were individually extracted and analyzed as described hereafter in order to determine: (1) trace organic compounds, specifically alkylamines, mono- and dicarboxylic acids, polycyclic aromatic hydrocarbons (PAHs), and n-alkanes; (2) water-soluble inorganic ions; and (3) organic carbon (OC) and elemental carbon (EC).

PM_{10} samples were analyzed for the determination of alkali metals and many transition elements.

2.2.1. PAHs and n-Alkanes

For PAHs and n-alkanes determination, a mixture of six deuterated PAH standards (acenaphthene-d10, phenanthrene-d10, fluoranthene-d10, benzo[a]anthracene-d12, benzo[a]pyrene-d12, dibenzo[a,h]anthracene-d14) was added to all filters as surrogate compounds to correct the data for the efficiency of extraction procedure. The filters were then extracted using 5.0 mL of dichloromethane (CH_2Cl_2 , purity $\geq 99.9\%$, Sigma-Aldrich) for 20 min in an ultrasonic bath. The extract was filtered (0.45 μm PTFE filter), the extraction solvent was evaporated under a gentle N_2 (99.999%, Sapio, Italy) stream. Finally, the residue was dissolved in 200 μL of isooctane (C_8H_{18} , purity $\geq 99.5\%$, for residue analysis, Honeywell Fluka™).

The PUF samples were extracted in a Soxhlet apparatus for about 6 hours (>20 cycles) with 250–300 mL of dichloromethane. The extract was concentrated by rotary evaporation (bath temperature ≈ 40 °C) until 4 mL. Then the extract was filtered using a PTFE syringe filter (0.45 μm ; Alltech, Nicholasville, KY, USA) to remove any insoluble particle and the solvent was further evaporated under a gentle N_2 (99.999%, Sapio, Italy) stream until dryness. Finally, the residue was dissolved in isooctane (purity $\geq 99.5\%$, for residue analysis, Fluka).

All the samples were analyzed using a GC-MS unit (GC 6850, MS 5973; Agilent Technologies, Santa Clara, CA, USA). The separation of the compounds was carried out on a ZB-XLB capillary column (length 60 m, i.d. 0.25 mm, film thickness 0.25 μm ; Zebron, Phenomenex, Torrance, CA, USA).

Helium (99.999%, Sapio, Italy) was used as carrier gas at a constant flow rate of 1 mL min⁻¹. A volume of 2 µL was injected in splitless mode by the autosampler. The MS operated in electron ionization mode (70 eV); the mass spectra were recorded in selected ion monitoring mode (SIM).

For the purpose of PAH determination, the injector was kept at 280 °C and the temperature program was from 80 °C to 330 °C. The transfer line was kept at 310 °C. Nineteen PAHs were determined in SIM mode by monitoring the mass/charge m/z corresponding to their molecular weight: naphthalene (NAPH), acenaphthylene (ACTY), acenaphthene (ACT), fluorene (FLN), phenanthrene (PHE), anthracene (ANT), fluoranthene (FLNT), pyrene (PYR), benzo[a]anthracene (BaA), ciclopenta[cd]pyrene (CPP), chrysene (CHR), benzo[b]fluoranthene (BbF), benzo[j]fluoranthene (BjF), benzo[k]fluoranthene (BkF), benzo[e]pyrene (BeP), benzo[a]pyrene (BaP), dibenzo[a,h]anthracene (DBahA), indeno[1,2,3-cd]pyrene (IcdP), and benzo[ghi]perylene (BghiP). It should be pointed out here that benzo[b]fluoranthene and benzo[j]fluoranthene co-eluted and they were determined together (BbjF). The average recoveries of deuterated PAHs spikes onto the filters were $37 \pm 5\%$ for acenaphthene-d10, $58 \pm 7\%$ for phenanthrene-d10, and $>60\%$ for the other deuterated standards. The PAH recoveries from the particulate matter were determined by analyzing three aliquots of standard reference material (SRM 1649a; NIST, Gaithersburg, MD, USA).

In order to quantify the n-alkanes, the injector was kept at 300 °C and the temperature program was from 60 °C to 300 °C. The transfer line was kept at 305 °C. The homologues series of 13 linear alkanes with 20–32 carbon atoms (C20–C32) were then determined by monitoring m/z 57, 71, and 85 during the whole chromatographic run. The n-alkane recoveries were estimated by spiking a standard mixture to a blank filter and extracting and analyzing it as a field filter; the recovery was full for every n-alkane. All the presented data were corrected for the described recoveries.

The external standard method was used for n-alkanes and PAHs quantification. Standard mixture of n-alkanes was prepared from single solid standards purchased from Alltech. A liquid standard mixture of PAHs was purchased from UltraScientific (Bologna, Italy).

Finally, a set of blank field filters (as stated above) for each sampling campaign were employed in order to evaluate the potential contamination of samples due to handling during the cruises and laboratory operations. For both PAHs and alkanes, the concentrations measured on the field filters were blank corrected; the values lower than the detection limit values on field filters were substituted by half of detection limit (dl) as suggested by Polissar et al. [83]. A more detailed description of PAHs and ALKs analysis is reported in Sangiorgi et al. [69].

2.2.2. PAHs Gas/Particle Partitioning

Due to the importance of PAHs in the environment, their phase partitioning was investigated. The gas-particle partitioning of a compound can be described through the distribution coefficient K_p :

$$K_p \text{ (m}^3 \text{ } \mu\text{g}^{-1}\text{)} = ((C_{ip}/TSP))/C_{ig} \quad (1)$$

where C_{ip} and C_{ig} are the concentration of the i -th compound in the particulate (p) and in the gaseous (g) phase, respectively, and TSP is the concentration of the total suspended particulate [84,85]. The phase partitioning may also be described by the fraction θ of a compound in the particulate phase:

$$\theta = C_{ip}/(C_{ip} + C_{ig}) \quad (2)$$

The gas/particle partitioning can be predicted using several models. According to the literature [69,85,86] the partitioning processes can be predicted using the absorption in the TSP OM and adsorption on TSP EC. It is the so called “dual model,” which is as follows:

$$K_p \text{ (abs + ads)} = 10^{-12} \left[\left(\frac{f_{OM}}{\rho_{OCT}} \times \frac{\gamma_{OCT} MW_{OCT}}{\gamma_{OM} MW_{OM}} \right) KOA + \left(f_{EC} \times \frac{a_{EC}}{a_{soot}} \right) KSA \right] \quad (3)$$

where f_{OM} is the TSP fraction of OM, and γ_{OCT} and γ_{OM} are the activity coefficients of the absorbing compound in octanol and TSP OM; MW_{OCT} and MW_{OM} are the molecular weight of octanol and TSP OM; and ρ_{OCT} is the density of octanol and KOA is the octanol–air partitioning coefficient. Equation (3) relates the absorption of a semi-volatile compound from air in TSP OM with its octanol–air partitioning coefficient. To be able to apply it, some values are needed. Assuming that octanol perfectly simulates the OM, it could be assumed that $\gamma_{OCT}/\gamma_{OM} = 1$. The molecular weight and density of octanol are 130 g mol^{-1} and 0.82 kg L^{-1} , respectively. Past applications usually assumed that the molecular weight of OM was the same of octanol. However, new reaction chamber experiments showed that it might be higher [87] and a MW of 500 g mol^{-1} is proposed [88], resulting in a ratio of $MW_{OCT}/MW_{OM} = 0.26$.

Finally, f_{EC} is the TSP fraction of elemental carbon (EC), a_{EC} and a_{soot} ($\text{m}^2 \text{ g}^{-1}$) are specific surface area of EC and soot, respectively, and KSA (L kg^{-1}) is the soot–air partitioning coefficient. The latter was calculated using a thermodynamic estimation model suggested by van Noort [89]:

$$\log KSA = -0.85 \log pL0 + 8.94 - \log (998/a_{soot}) \quad (4)$$

The dual model assumes that the EC accounts for the majority of soot, then $a_{EC}/a_{soot} = 1$ [86]. KSA for PAHs were calculated using Equation (4), using the range values for a_{soot} of 59.1 and $370 \text{ m}^2 \text{ g}^{-1}$ suggested in Dachs et al. [86]. The dual model also uses octanol as a surrogate of OM in the absorptive partitioning and EC as a surrogate for soot in the adsorption process. Considering the aforementioned assumptions, Equation (3) becomes:

$$Kp (abs + ads) = 10^{-12} \times KOA \times f_{OM} \times 0.32 + KSA \times f_{EC} \quad (5)$$

Equation (5) was successfully applied to PAHs by some authors [66,69,70,90].

In order to predict the partitioning coefficient, $Kp (abs + ads)$, for semi-volatile PAHs, we used the recommended values of KOA reported in Ma et al. [64]. As suggested by Lohmann and Lammel [85] all the measured $\log Kp$ should be reported to 298 K using in order to ensure the comparability between sample collected under various atmospheric conditions as follows:

$$\log Kp (298K) = \log Kp (T) + [\log pL (T) - \log pL (298K)] \quad (6)$$

Finally, the same approach was also used for ALKs gas/particle partitioning as detailed in Sangiorgi et al. [69].

2.2.3. Water-Soluble Compounds

Water-soluble inorganic ions, carboxylic acids, and alkylamines were determined by extracting the collected filter samples three times each, in a total of 3.0 mL of ultrapure water (1.0 mL each time; 18.2 M Ω cm resistivity, Milli-Q system; Millipore, Billerica, MA, USA) for a total of 30 min (10 min each time) in an ultrasonic bath (SONICA[®]; Soltec, Milan, Italy). The extracts were then filtered (0.45 μm PTFE filters; Alltech, Nicholasville, KY, USA) to remove insoluble fractions and analyzed by an ion chromatography system (Dionex ICS-2000; Dionex, Sunnyvale, CA, USA) equipped with an electrical conductivity detector. For the analysis of inorganic cations (Na^+ , NH_4^+ , K^+ , Mg^{2+} , Ca^{2+}) as well as alkylamines (methylamine, dimethylamine, trimethylamine, ethylamine, diethylamine, triethylamine), an Ion Pac CG17 (4 \times 50 mm) guard column and an Ion Pac CS17 (4 \times 250 mm) analytical column were used together with a CSRS 300 (4 mm) electrolytic suppressor. An elution gradient of Methanesulfonic Acid (MSA) from 3 to 40 mM was used with a constant flow rate of 1.0 mL/min. The column and detector cell temperatures were both kept at 50 $^\circ\text{C}$. For the analysis of inorganic anions (F^- , Cl^- , NO_3^- , SO_4^{2-}) as well as mono- and dicarboxylic acids (formate, acetate, propionate, oxalate, malonate, succinate, glutarate), an Ion Pac AG11 (4 \times 50 mm) guard column and an Ion Pac AS11 (4 \times 250 mm) analytical column were used together with an ASRS-ultra II (4 mm) electrolytic suppressor [26]. An elution gradient of KOH from 0.1 to 50 mM was used with a

constant flow rate of 0.8 mL/min. The column and detector cell temperatures were kept at 30 °C and 35 °C, respectively. Quantification was made by using the external standard method. Single liquid standards (1 g L⁻¹; Fluka, Sigma-Aldrich, St. Louis, MO, USA) were used for inorganic ions and solid pure standards were used for alkylamines and carboxylic acids (pure grade >99.5%; Chemie GmbH, Sigma Aldrich).

2.2.4. OC, EC, and Metals

OC and EC were determined by means of a carbon analyzer (Sunset Laboratory, Tigard, OR, USA) using the NIOSH (National Institute for Occupational Safety and Health) 5040 protocol [91].

Trace elements, including rare earth elements (REEs) were also measured using a high resolution ICP-MS (Inductively Coupled Plasma-Mass Spectrometer) technique on PTFE aerosol samples (PM₁₀) collected during AREX 2011 cruise at a 12 h resolution. The analytical determinations were carried out using an ELEMENT2 (Thermo Fisher Scientific, Waltham MA, USA) system consisting of a double focusing magnetic sector field inductively coupled plasma mass spectrometer (ICP-SF-MS) equipped with a reverse Nier-Johnson geometry and coupled with a desolvation system provided with a microflow nebulizer. The use of a mass spectrometer detector was pivotal in order to measure accurately very low concentration levels [77].

2.3. Back Trajectories and Copernicus Atmosphere Monitoring Service Data

Five-day, air mass back trajectories were derived in 6 h intervals using the hybrid single particle Lagrangian integrated trajectory model (4.8) developed by the National Oceanic and Atmospheric Administration Air Resource Laboratory (<http://ready.arl.noaa.gov/HYSPLIT.php>). Each back trajectory was determined at 100 m, 500 m, and 1000 m above the sea level. They are reported in supporting information (Figures S1 and S2) and were simply used to interpret the averaged chemical composition of the AREX2011 and AREX2012 campaigns.

Finally, the Copernicus Atmosphere Monitoring Service (CAMS) [92] was used to obtain the aerosol optical depth (AOD), in terms of aerosol species, in order to compare them with the experimental chemical composition determined close to sea surface. This was done with the aim: (1) to verify if the interannual variation of the columnar optical properties was in agreement with chemical composition measured at ground, and (2) to highlight any difference between ground-base and columnar data in terms of relative contribution of each aerosol species to the total, in order to highlight the need of vertical aerosol profiles over the open Arctic Ocean.

In this respect, it has to be recalled that a crucial role on the climatic response of aerosol is played not only by the aerosol species concentrations, but also by their vertical aerosol distribution, as recently reported in Ferrero et al. [32]. In fact, the same type of aerosol can produce different climatic effects (warming or cooling) and local feedbacks (snow/ice albedo, clouds) depending on its vertical location [3,19,29].

CAMS provides reanalysis of the AODs (550 nm) and atmospheric aerosol composition for five types of tropospheric aerosol particles: sea salt, sulphates, dust, black carbon, OM [93]. CAMS embeds the Monitoring Atmospheric Composition and Climate-Interim Implementation (MACC-II), which is based on data of the European Centre for Medium-Range Weather Forecast (ECMWF) [94]. For the purpose of the present application (in the middle of the Arctic Ocean), the dust output was not considered.

3. Results

As expected in the Arctic area, particulate matter concentrations were very low. The average TSP concentrations were 4.2 ± 2.8 and 7.7 ± 2.5 $\mu\text{g m}^{-3}$ during the summers of 2011 and 2012, respectively. The detection limits, calculated as the average of blank filters plus three times the standard deviation, were $1.2 \mu\text{g m}^{-3}$ and $1.0 \mu\text{g m}^{-3}$ during 2011 and 2012 campaign, respectively, ensuring the reliability of the obtained data. Moreover, as TSP and PM₁₀ concentrations were determined at the same time during

AREX2011, they were compared; results reported in Figure 3 that shows a good linear correlation ($R^2 = 0.760$, $n = 19$) with a slope of 0.915 in agreement with the fact that PM_{10} is only a fraction of the TSP. This result stresses the accuracy of the particulate matter measurements carried out along the cruise. Moreover, some scattering between TSP and PM_{10} could be due to the different origins of marine aerosol: primary film drops and secondary aerosol, due to their inner nature, contained both TSP and PM_{10} , while jet drop aerosol could be found only in TSP [95].

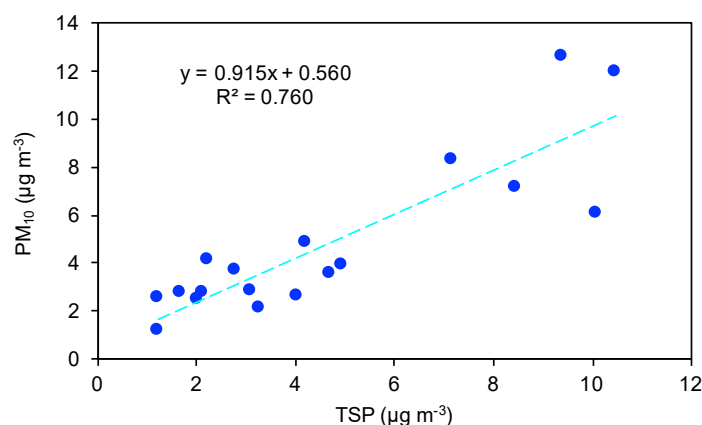


Figure 3. Linear correlation between PM_{10} and TSP during AREX2011 ($n = 19$).

The chemical analysis carried out on the aforementioned samples revealed that, on average, the collected samples were composed of water-soluble compounds and carbonaceous material for more than 90% of the particle mass. Thus, within the following sections (Section 3.1, Section 3.2, and Section 3.3), the chemical composition is detailed following the mass fraction explained by each chemical group. The results start focusing on the water-soluble compounds (Section 3.1) and the carbon content (Section 3.2); their concentrations (averaged along AREX 2011–2012 cruises) are reported in Table 1 together with the chemical composition determined at the same time in Ny-Ålesund (Gruvebadet site; Section 1). PAHs and ALKs results follow in Section 3.3 and finally, element concentrations in Section 3.4. All averaged data are reported as mean \pm mean standard deviation.

Table 1. Average values in $ng\ m^{-3}$ (and mean standard deviation) of inorganic ions, OM, EC, carboxylic acids, and amines determined during the summers of 2011–2012, both along the AREX cruise and in Ny-Ålesund (Grivebadet station); * indicates that the concentrations reported for both carboxylic acids and amines are also part of the OM concentration while - - indicates the chemical species not determined in Ny-Ålesund.

Compound	AREX2011–2012		Ny-Ålesund (2011–2012)	
	Mean	σ_m	Mean	σ_m
Cl^-	1851	716	239	23
Na^+	1138	348	161	14
SO_4^{2-}	637	199	110	7
NO_3^-	95	40	32	3
NH_4^+	47	32	24	2
K^+	42	14	7	1
Mg^{2+}	125	47	18	1
Ca^{2+}	105	37	13	1
OM	1948	255	621	13
EC	30	2	--	--
glut *	7	2	--	--
succ *	7	5	--	--
oxa *	19	6	5	1
DMA *	4	1	--	--
TMA *	2	1	--	--
DEA *	1	1	--	--

3.1. Water-Soluble Species

3.1.1. Water-Soluble Inorganic Ions

Na^+ , NH_4^+ , K^+ , Mg^{2+} , and Ca^{2+} cations and Cl^- , NO_3^- , and SO_4^{2-} anions were detected on the filter samples. Their concentrations during AREX2011 and AREX2012 are reported in Figure 4 (and summarized in Table 1).

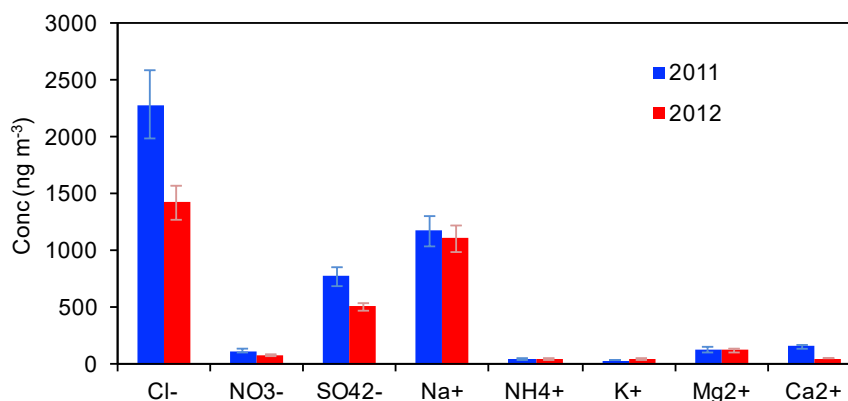


Figure 4. Average concentration values of inorganic ions detected both during AREX2011 and AREX2012.

From these data, the contribution of sea salt to these species was calculated using a set of equations available in literature and dedicated to this purpose. First, the sea salt aerosol concentration was calculated referring to Bates et al. [96]:

$$\text{sea salt} \left[\mu\text{g}/\text{m}^3 \right] = \text{Cl}^- \left[\mu\text{g}/\text{m}^3 \right] + 1.47 \times \text{Na}^+ \left[\mu\text{g}/\text{m}^3 \right] \quad (7)$$

where 1.47 is the mass ratio of the sum of Na^+ , K^+ , Mg^{2+} , Ca^{2+} , SO_4^{2-} , and HCO_3^- to Na^+ in sea water. This approach was followed as it presents the advantage to avoid the inclusion of non-sea-salt (nss-) K^+ , Mg^{2+} , Ca^{2+} , and SO_4^{2-} , and allows, at the same time, to consider the loss of Cl^- due to the Cl^- depletion processes [97,98]. Finally, the sea salt contribution to the observed concentrations of K^+ , Mg^{2+} , Ca^{2+} , Cl^- , and SO_4^{2-} were determined following Mihalopoulos et al. [99]:

$$\text{ss}_X \left[\mu\text{g}/\text{m}^3 \right] = \frac{X}{\text{Na}^+} \times \text{Na}^+_{\text{measured}} \left[\mu\text{g}/\text{m}^3 \right] \quad (8)$$

where X is the selected species and X/Na^+ is the mass ratio of its concentration to that of Na^+ in the sea water as reported in References [100,101].

The average concentration of sea salt aerosol was $3.5 \pm 1.2 \mu\text{g m}^{-3}$ with higher values during 2011 ($4.1 \pm 2.2 \mu\text{g m}^{-3}$) compared to 2012 ($3.0 \pm 1.3 \mu\text{g m}^{-3}$). This interannual behavior should be explained considering the average wind speed close to the surface (10 m) along the cruises: 5.6 ± 0.4 and $4.5 \pm 0.5 \text{ m s}^{-1}$ during 2011 and 2012, respectively. As a matter of fact, the ocean may act as a primary direct source of aerosol as a result of turbulence at the surface, e.g., related to bubble-bursting emissions [96]. Moreover, an important result comes out when comparing (at the same time) the sea salt concentrations measured along the cruises with those measured over land in Ny-Ålesund (Table 1): the sea salt concentrations were systematically 7 times lower ($\approx 1\text{--}3 \mu\text{g m}^{-3}$ less) over land. The data recorded at the Gruevbadet station were in agreement with those reported in previous works (e.g., Udisti et al. [35]). Interestingly, AREX2011 and AREX2012 sea salt data were in agreement with the sea salt aerosol concentrations measured over sea in the Southern Ocean ($5.9 \pm 5.6 \mu\text{g m}^{-3}$) and coastal East Antarctica ($2.6 \pm 2.3 \mu\text{g m}^{-3}$) [102].

Going into details regarding sea spray, Figure 5 reports the sea salt percentage of the major inorganic ions detected during both cruises. Almost all the Cl^- and Mg^{2+} and most of the K^+ derived from sea salt aerosol with mean values of $94 \pm 4\%$, $97 \pm 4\%$, and $79 \pm 15\%$, respectively. Both, SO_4^{2-} and Ca^{2+} were also associated with a nss- origin.

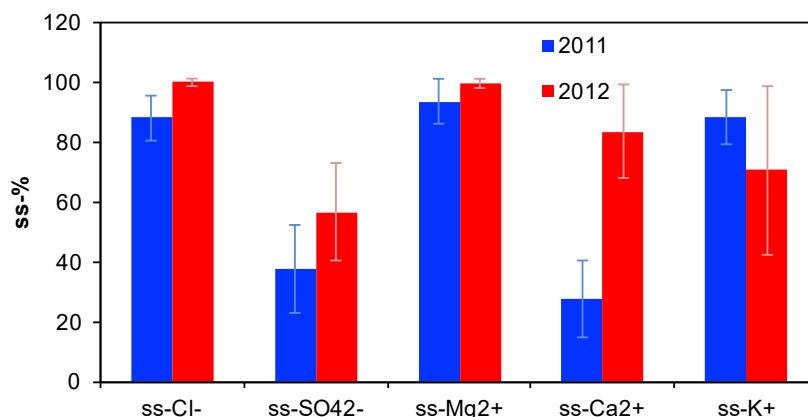


Figure 5. Average sea salt percentage of the major inorganic ions detected both during AREX2011 and AREX2012.

Such a behavior could be first explained by the 2011 and 2012 back trajectories calculated using HYSPLIT (Section 2.3 and Figures S1 and S2, Supplementary Material). In fact, air masses travelled over Iceland and close to Greenland and they can transport crustal material in TSP enriched in gypsum (CaSO_4) as demonstrated by Moroni et al. [103,104]. Moreover, it has to be underlined that a part of nss- SO_4^{2-} may derive from the conversion, into the atmosphere, of dimethylsulfide (DMS) which is produced in surface seawater from the enzymatic cleavage of dimethylsulfonium propionate [105]. In fact, not only primary emissions (i.e., sea spray) are important, but also secondary ones, as a result of the secondary reaction on precursors emitted by the sea into the atmosphere [106]. The average concentration of nss- SO_4^{2-} was $363 \pm 140 \text{ ng m}^{-3}$ (2011: $459 \pm 187 \text{ ng m}^{-3}$; 2012: $266 \pm 209 \text{ ng m}^{-3}$). Even these records were ≈ 9 times higher with respect to those simultaneously measured at Gruebadet [35], and $\approx 100\text{--}200 \text{ ng m}^{-3}$ higher than those reported both at Zeppelin (<http://ebas.nilu.no>) and Alert (Greenland) stations [107]. Similar summertime concentrations of nss- SO_4^{2-} were found by Xu et al. [102] and by Minikin et al. [108] over the Southern Ocean indicating high marine biogenic emissions.

For NO_3^- (Figure 4), the average concentration was $95 \pm 46 \text{ ng m}^{-3}$ (2011: $117 \pm 78 \text{ ng m}^{-3}$; 2012: $73 \pm 51 \text{ ng m}^{-3}$), 3 times higher than in Ny-Ålesund (Table 1) and ≈ 2 times with respect to those reported by Xu et al. [102] ($41 \pm 8.0 \text{ ng m}^{-3}$ over the Southern Ocean and of $50 \pm 20 \text{ ng m}^{-3}$ over coastal East Antarctica). This was especially true for 2011 campaigns, when more air masses originated from Europe and Russia (Figure S1). In this respect, the north to south difference was in keeping with carboxylic acid behavior discussed in Section 3.1.2, suggesting their continental sources from secondary (photochemical) production from precursors (e.g., NO_x) during long-range transport (as the North Hemisphere is more affected by anthropogenic settlement).

Lastly, the average concentration of NH_4^+ was $47 \pm 33 \text{ ng m}^{-3}$ (2011: $47 \pm 59 \text{ ng m}^{-3}$; 2012: $46 \pm 30 \text{ ng m}^{-3}$), 2 times higher than in Ny-Ålesund (Table 1) but in keeping with $42 \pm 31 \text{ ng m}^{-3}$ over the Southern Ocean [102]. The long-range transport of substances from the continents (mid-latitude) could be the primary source of ammonium in aerosols; however, some NH_3 can be emitted from seabirds [109,110]. In this respect, several authors [109,111] estimated that NH_3 emissions from seabirds can explain 1.8–2.7% of oceanic emissions converted into ammonium. The air–sea exchange of NH_3 (enabling the formation of secondary marine aerosols) has long been recognized [112,113].

All of these results highlight the importance of carrying out experimental measurements in open seas where the relative importance of an aerosol source (e.g., the sea spray, emission of biogenic

precursors) can be better and fully captured than over land, where local micrometeorology can play an important role [32,80]. Long-term land-based measurements and intensive observational campaigns (cruise-based) become a complementary source of information concerning aerosol chemical composition in the Arctic.

3.1.2. Water-Soluble Organic Ions

Data concerning the water soluble organic compounds over the Arctic Ocean are less recognized and reported, and there are few important data series (land-based) [43]. Figure 6 reports their concentrations measured during ATEX2011 and ATEX2012, and below the carboxylic acid behavior is discussed first, followed by that of amines.

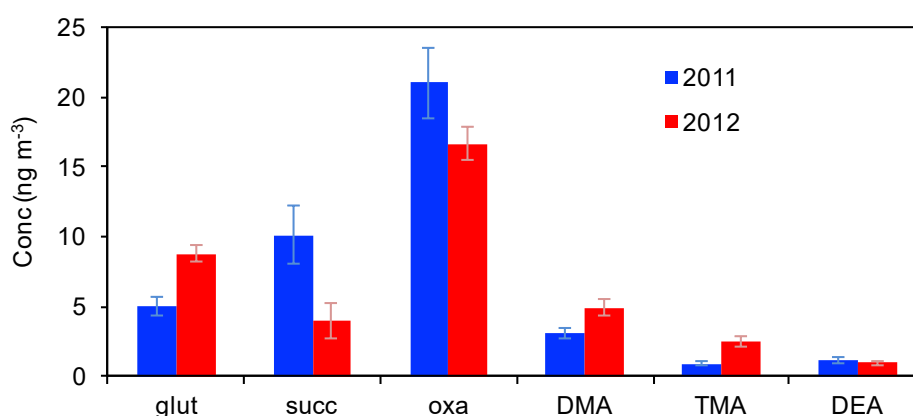


Figure 6. Concentrations of organic ions during ATEX2011 and ATEX2012: glutaric (glut), succinic acids (succ), oxalic acid (oxa), dimethylamine (DMA), trimethylamine (TMA), and diethylamine (DEA).

Starting with carboxylic acid, the average concentration of oxalic acid during ATEX cruise was $17 \pm 6 \text{ ng m}^{-3}$ (2011: $19 \pm 11 \text{ ng m}^{-3}$; 2012: $14 \pm 4 \text{ ng m}^{-3}$), while succinic and glutaric were lower: $6 \pm 2 \text{ ng m}^{-3}$ and $6 \pm 5 \text{ ng m}^{-3}$, respectively. Thus, the oxalic acid was the dominant dicarboxylic acid (about 60%), while the other two detected, glutaric (glut) and succinic acids (succ), were about 20% for each one. For the oxalic acid (the only one measured in Ny-Ålesund), it was found to be 4 times higher than at the Gruevbadet site. This is in agreement with Xu et al. [102] who found that isoprene emitted by marine photosynthetic organisms is the major source of oxalic acid in the marine boundary layer as also reported by Kawamura and Ikushima [114]. In fact, the aforementioned data are closer to those measured by Kawamura et al. [51] over the Arctic Ocean: $8.48 \pm 3.87 \text{ ng m}^{-3}$ for oxalic acid $4.59 \pm 1.44 \text{ ng m}^{-3}$ for succinic acid and $0.59 \pm 0.58 \text{ ng m}^{-3}$ for glutaric acid. Conversely, they are higher than those reported by Xu et al. [102]: $3.8 \pm 3.8 \text{ ng m}^{-3}$ of oxalate over the Southern Ocean and of $2.2 \pm 1.5 \text{ ng m}^{-3}$ over coastal East Antarctica (and even lower values for succinate: $0\text{--}2.9 \text{ ng m}^{-3}$ over the Southern Ocean and of $0\text{--}0.95 \text{ ng m}^{-3}$ over coastal East Antarctica).

This north to south difference in carboxylic acid concentrations was yet explained by Kawamura [51] who found an enrichment of diacids over the Arctic Ocean when air masses arrived from the continents, thus suggesting their continental sources including polluted urban aerosols [114] and secondary (photochemical) production from various organic precursors (e.g., isoprene and other biogenic volatile organic compounds (VOCs)) during long-range transport. As the North Hemisphere is more affected by anthropogenic settlement, this could explain the difference and support the obtained data. Moreover, ATEX2011 campaign showed highest oxalic acid and succinic acid concentrations than those measured during ATEX2012. A possible explanation is related to the air mass origins during the two campaigns (2011–2012 back trajectories in Figures S1 and S2, Supplementary Material); during 2011 more air masses travelled over Europe and northern Russia than during 2012.

Concerning the amines, their atmospheric concentration were completely negligible compared to the other water-soluble compounds (Table 1, Figures 4 and 6). Particularly, only dimethylamine

(DMA), trimethylamine (TMA), and diethylamine (DEA) were detected. Averaging the two campaigns, their concentrations were: 3.98 ± 1.21 , 1.70 ± 0.82 , and $1.06 \pm 0.56 \text{ ng m}^{-3}$. These values are very important because they are close to those used by Almeida et al. [40] to simulate (in the CLOUD chamber experiment) the ambient nucleation rate in a H_2SO_4 -DMA- H_2O system, finding out that nucleation rates with 5 p.p.t.v. (parts per trillion by volume) DMA were enhanced more than 1000-fold compared with 250 p.p.t.v. ammonia (H_2SO_4 - NH_3 - H_2O system). Moreover, as reported in literature [115–117], low temperature conditions decrease the height of the barrier for new particle formation even considering the very simplified binary H_2SO_4 - H_2O system, thus again underlying the importance of the detected amines in polar regions. The importance of the previous findings is also highlighted by the nss-SO_4^{2-} values reported in Section 3.1.1 that may underline a secondary origin of aerosol in the atmosphere.

Finally, aerosol acidity was estimated from the whole water-soluble composition by correlating the anion and cation charges in terms of equivalents (Figure 7). Results were characterized by good linear correlations ($R^2 = 0.961$ and $R^2 = 0.922$ during AREX2011 and AREX2012, respectively) with slopes close to one (1.041 and 0.994 during AREX2011 and AREX2012, respectively). These data highlight that the collected aerosol samples were close to neutrality.

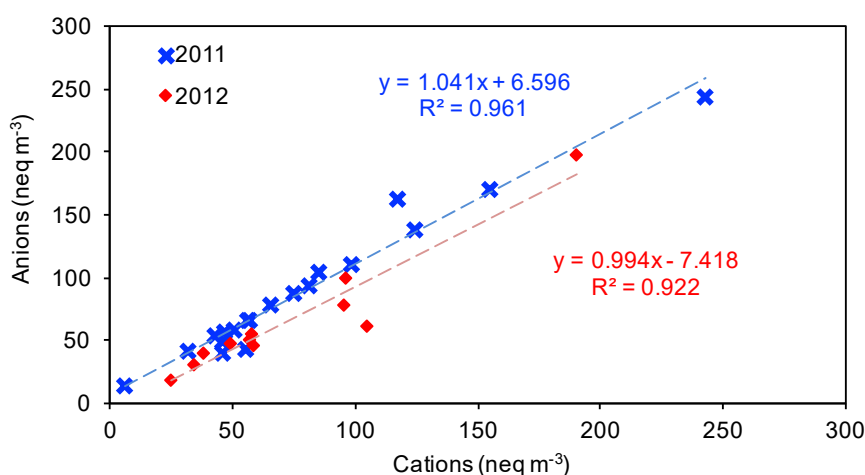


Figure 7. Linear correlations between the concentrations (expressed as neq m^{-3}) of cations and anions determined both during AREX2011 ($n = 19$) and AREX2012 ($n = 14$).

3.2. Carbonaceous Material And Full Chemical Composition

Average concentrations of total carbon in the collected samples were 1114 ± 150 and $802 \pm 191 \text{ ng m}^{-3}$ during 2011 and 2012, respectively. The organic fraction accounted alone for more than 95% of total carbon and the remaining 5% was due to EC that accounted on average for 35 ± 1 and $25 \pm 1 \text{ ng m}^{-3}$ during 2011 and 2012, respectively.

When the OC was converted to OM (using a factor of 2.1 in remote Arctic regions [32]) the values increased up to 2265 ± 315 and $1631 \pm 400 \text{ ng m}^{-3}$ during 2011 and 2012, respectively.

These data are first in agreement first with the average concentration of the total carbon measured over the Arctic Ocean by Kawamura et al. [118]. However, OM was found to be considerably higher over the sea (by a factor of 3) compared to the land-based measurements in Ny-Ålesund (Table 1). Instead, the EC concentrations are close to the equivalent black carbon concentrations measured during the last AREX2018 cruise (personal communication from the scientific chief of the expedition). As reported in Yttri et al. [119], $8.8 \pm 4.5 \%$ of EC in the Arctic can be originated by biomass burning, which is a source also connected with brown carbon and PAHs [57] (PAHs are presented in Section 3.3).

Higher OM and EC during 2011 are in agreement with the results and chemical markers reported in the previous Section 3.1 and with back trajectories in Supplementary Material (Figures S1 and S2).

Given the organic material concentration it is possible to determine the relative contribution of the major constituents of the TSP collected along the cruise: by the following chemical components: OM (30.5%), Cl^- , (29.0%), Na^+ (17.8%), SO_4^{2-} (10.0%), the other ions (6.5%), and finally EC (0.5%). These data are presented in Figure 8a while Figure 8b reports the same relative contributions in Ny-Ålesund.

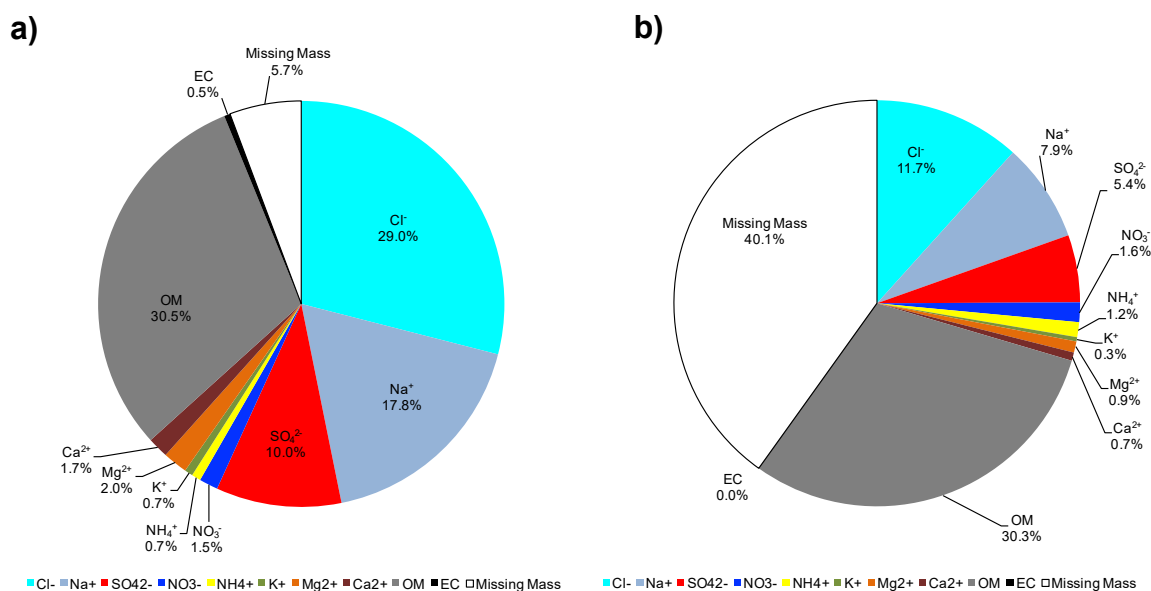


Figure 8. Relative contributions (percentages) of the major constituents of the aerosol samples collected: (a) along the cruise, and (b) in Ny-Ålesund. Missing mass indicates the aerosol mass fraction not explained by the chemical components that were analyzed.

It is noteworthy in Figure 8a that the OM content in open sea was very high (30.5%), close to that of Cl^- ; this may suggest the importance of the biological emission from the sea as yet suggested from the amines results. The analysis of n-alkanes behavior (Section 3.3) is aimed to strengthen this point.

Results reported in Figure 8a,b clearly show that over the sea, the total aerosol concentration can be explained by the water soluble species and the carbon fraction (the missing mass was only 5.7%); conversely, in Ny-Ålesund, a huge fraction of aerosol mass was not explained by the classical chemical analysis. The missing mass reached 40.1% in keeping with data reported in Ferrero et al. [32]. This should be an indication of the presence of mineral compounds (related to dust) as described in Moroni et al. [103,120].

This stresses again the importance of intensive observational campaigns (cruise-based) as a complementary source of information concerning the aerosol chemical composition in the Arctic.

In addition to this, it has to be recalled that both land-based and cruise-based data (apart from the Zeppelin station) are close to sea level, while also the vertical aerosol location is fundamental to reveal the aerosol climatic effects [3,19,29]. Therefore, the CAMS data were used here to estimate the columnar AOD in function of different aerosol components (Section 2.3). Even though aerosol chemistry was measured at sea level, results were used to highlight the multi-annual behavior and also to derive indication on the vertical importance of different species with respect to the ground-level.

Figure 9 presents the comparison between CAMS-AOD and aerosol chemistry from AREX cruises concerning the amount for: sea salt, OM, EC, and sulfates (CAMS data corresponding to each aerosol samples are reported in Table S1, Supplementary Material). Starting with the interannual trend, it appears that all the species were more concentrated in 2011. Particularly, going from 2011 to 2012, a decrease of 27%, 28%, 27%, and 35% was observed (from chemical analysis) for sea salt, OM, EC, and sulfates, respectively; CAMS results were fully in agreement leading to a AOD decrease (for the same species) of: 21%, 26%, 22%, and 40%, respectively.

Moreover, Figure 9 shows a higher contribution of sulfates to the columnar AOD (47%), despite at the ground-level they chemically accounted only for 10.0% (Figure 8a); this could indicate a higher importance of transport and secondary formation of sulfates at higher altitudes and stress the importance of coupling future ship measurements with vertical profile investigations. In this respect, the future AREX campaign will couple ship-based measurements with an unmanned aerial vehicle (UAV)-based optical measurements to perform vertical profiles over the Arctic Ocean.

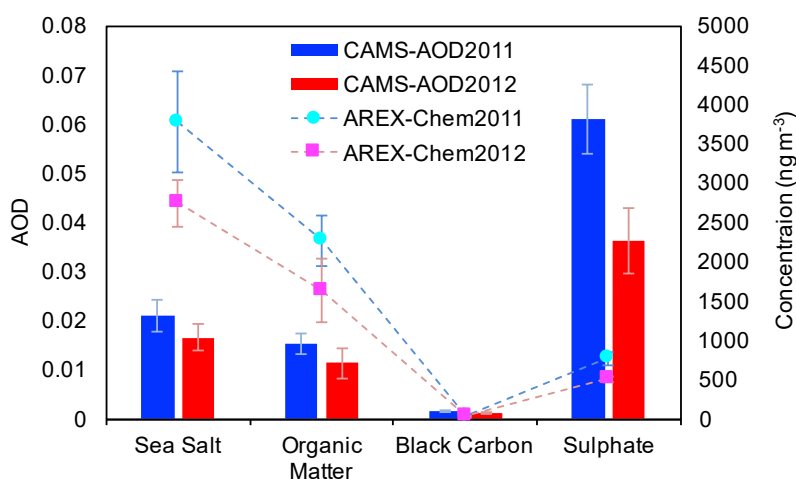


Figure 9. CAMS AOD and AREX2011–2012 chemical concentrations for sea salt, OM, EC, and sulfates.

3.3. PAHs and *n*-Alkanes

3.3.1. PAHs

Eighteen PAHs were analyzed in TSP samples; among them, the most abundant ones were the semi-volatile PAHs: together they accounted for 80% of all the PAHs. On average, phenanthrene was $35 \pm 6\%$ of all PAHs, fluoranthene $21 \pm 4\%$, pyrene $13 \pm 3\%$, fluorene $11 \pm 3\%$, and chrysene $8 \pm 2\%$. All the other PAHs were found in the order of magnitude of 1 pg m^{-3} . Their pattern is repeated in Figure 10, from which it is also evident that the concentration of PAHs was higher during the summer of 2011 ($20.4 \pm 11.0 \text{ pg m}^{-3}$) than the summer of 2012 ($8.2 \pm 3.3 \text{ pg m}^{-3}$). This behavior was mainly related to semi-volatile compounds (from FLN to CHR). It is possible to neglect a temperature influence as it was essentially the same (6.5 ± 1.4 and 6.0 ± 0.8 °C), both during AREX2011 and AREX2012, respectively. Thus, as described for the dicarboxylic acids, a possible explanation is related to the air masses origin during the two campaigns (Figures S1 and S2): during 2011, a large number of air masses travelled over Europe and northern Russia, while during 2012, essentially pure Arctic air was sampled. Even when considering 2011, the PAHs concentrations were about an order of magnitude lower than those recorded over the Mediterranean Sea [121]. Despite this, their fate in the Arctic is very important as PAHs are classified as POPs, thus accumulating into the environment, especially in cold areas. The total (particulate + gaseous) concentrations were $447.5 \pm 254.1 \text{ pg m}^{-3}$; higher concentrations were found in other studies (Mediterranean Sea [121]: $0.5\text{--}2.6 \text{ ng m}^{-3}$; Canadian Arctic [122]: $38\text{--}392 \text{ pg m}^{-3}$). The PAHs in the gas phase (volatile and semi-volatile regime from NAPH to CHR) were much higher than the particulate phase, ranging from 163 to 1136 pg m^{-3} and were similar to those measured in the Canadian Arctic from 1993 to 2000 (113 to 516 pg m^{-3}) [122]. Thus, the gas phase PAHs dominated the total PAHs in the volatile/semi-volatile regime; conversely, within the non-volatile regime, PAHs were only in particulate matter phase with a concentration of $1\text{--}2 \text{ pg m}^{-3}$. The aforementioned observations were also fully in agreement with the reported data (since 1994) at the Zeppelin station (Svalbard) [59,123], where the volatile PAHs (e.g., naphthalene and fluorene) were found as dominant ones. Most importantly, they highlighted that the more volatile PAHs are more abundant towards the Arctic (by comparing PAHs at Zeppelin and Andøya stations in Northern

Norway). PAHs behavior was investigated by dividing the ship route in two main parts: 71–76° N (between Norway and Svalbard) and 76–80° N (around and above Svalbard). Semi-volatile PAHs concentrations (from FLN to PYR) were found to be 2.3 ± 0.5 and 1.7 ± 0.4 times higher in particle and gas phases, respectively, in the northern track of the ship, in keeping with the literature data.

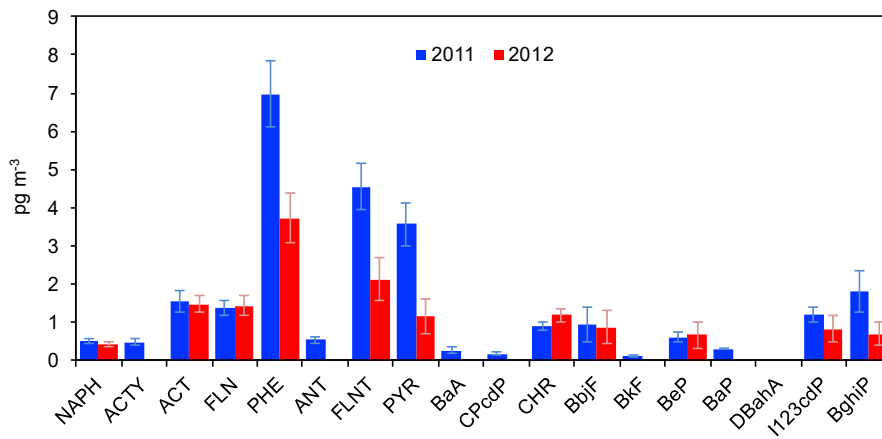


Figure 10. PAHs pattern in particulate matter phase during both AREX2011 and AREX2012.

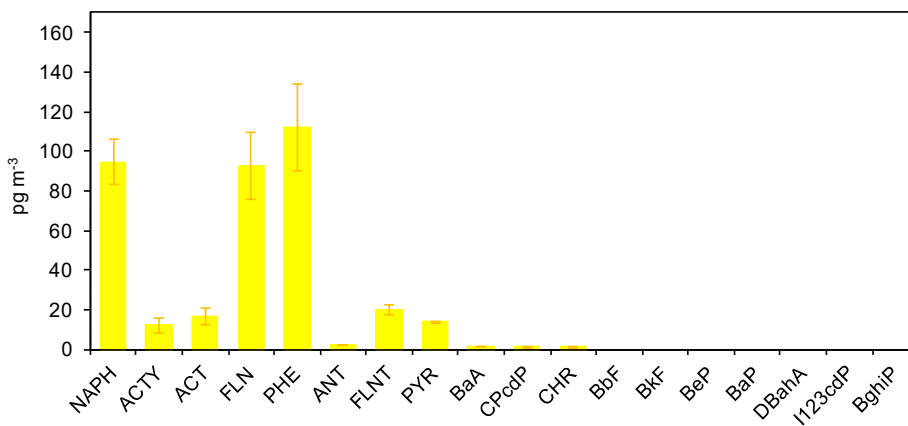


Figure 11. PAHs pattern in gas phase during AREX2011.

Using the data reported in Figures 10 and 11, the PAHs partitioning was investigated. The experimental and predicted Kp were calculated for semi-volatile PAHs (from FLN to CHR) following the approach of Sangiorgi et al. [69] described in Section 2.2.4. Results are reported in Figure 12a,b, from which it is evident that the Kp values spread around the 1:1 line ($R^2 = 0.609$) suggesting an ambient equilibrium of PAHs phase-partitioning; in fact, if the data are averaged (along the whole cruise) for each PAH species (Figure 12b), the linear correlation between the experimental and predicted Kp reach high values ($R^2 = 0.971$) with a slope close to one (1.250).

This result is in agreement with the fact that PAHs are anthropogenic substances that, first, can be transported far from the source location, and second (and most importantly), whose fate is related to chemical composition of the particles that are able to influence their phase partitioning.

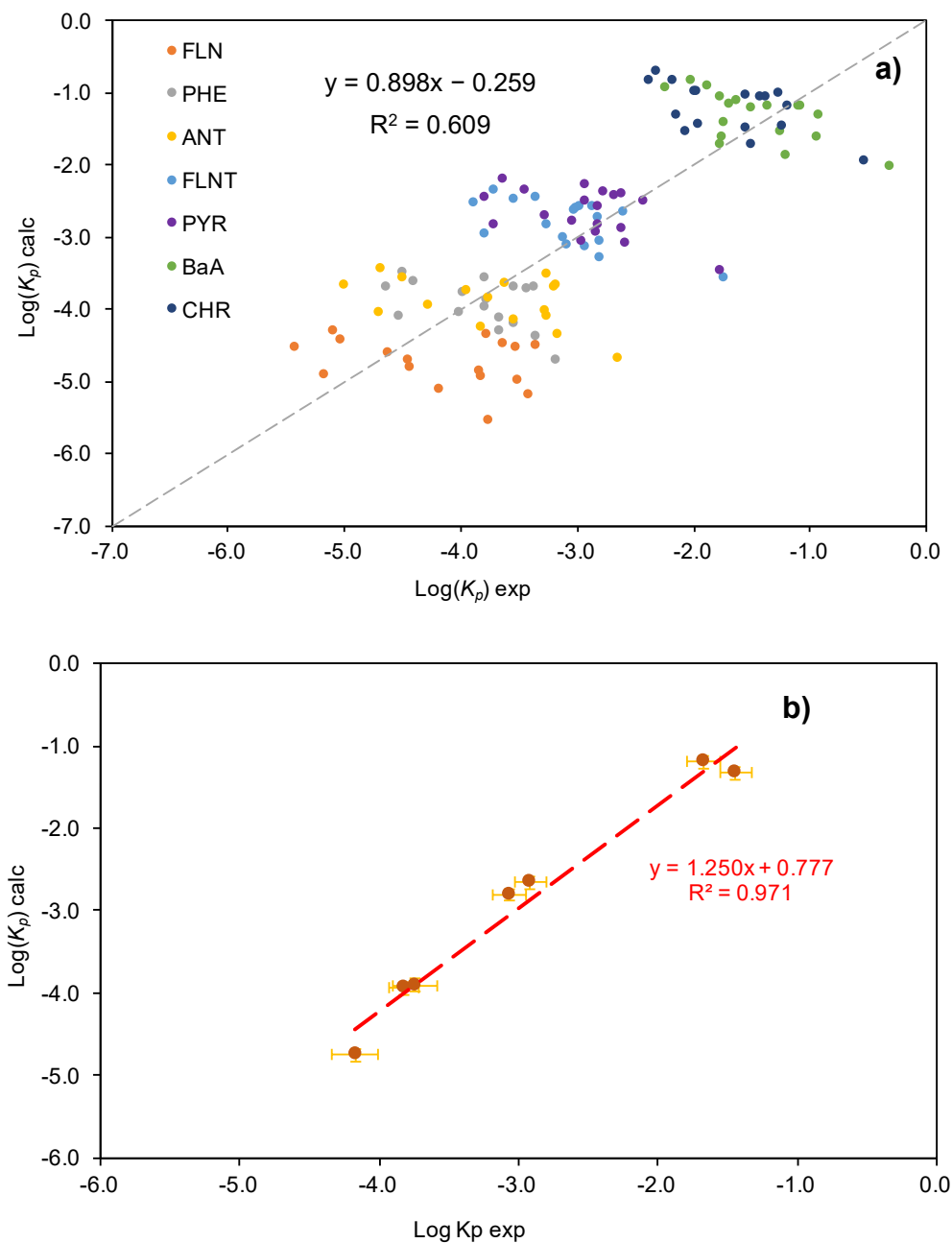


Figure 12. Experimental vs predicted K_p for semi-volatile PAHs (from FLN to CHR) for: (a) each collected sample and PAH species ($n = 133$); (b) each PAH species averaged along the cruise ($n = 7$).

3.3.2. Alkanes

As for the ALKs, the most abundant ones were those with 24–32 carbon atoms. The average concentration of each single ALK ranged between 20 pg m^{-3} (C21) to 500 pg m^{-3} (C29) (Figure 13) while the total ALKs particulate phase concentrations ranging from 0.5 to 3.2 ng m^{-3} . Similar values (0.14 – 4.5 ng m^{-3}) were measured by Fu et al. over the Arctic Ocean [124], while higher concentrations were measured at the Svalbard Islands [125] (19 – 97 ng m^{-3}). The relative abundance of n-alkanes to OC in aerosols was $0.16 \pm 0.06\%$.

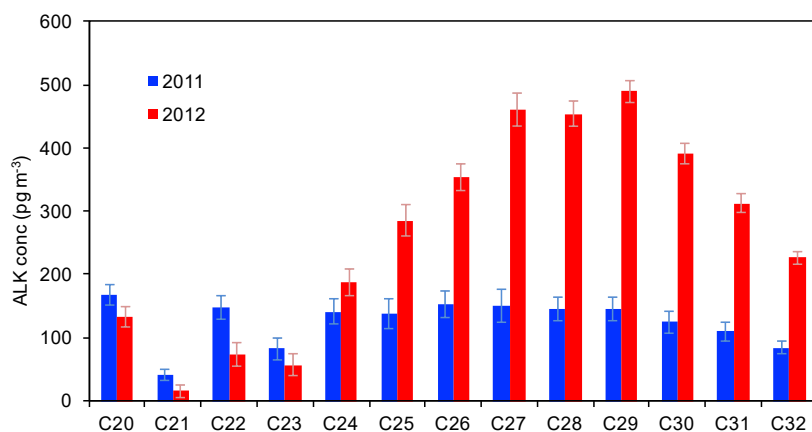


Figure 13. ALKs pattern in particulate matter phase during both ATEX2011 and ATEX2012.

As reported in Marty and Saliot [41], a useful parameter to describe the ALKs is the carbon preference index (CPI), which is calculated as a ratio of the sum of concentrations of the odd versus the even numbered carbon ALKs. In fact, the CPI can be used as a tracer of the origin (anthropogenic, marine, terrestrial) of the particulate matter organic fraction [41]. Over the sea, CPI can reach values close to 1 or lower as n-alkanes do not show a characteristic input from phytoplankton sources; Stortini et al. [42] reported that marine organisms can exhibit odd/even ratios both more and less than 1, showing that CPI values are always lower than 1 for both particulate and dissolved fractions. Phytoplankton cultures can have higher C15 or C17 (not measured in this study) abundance with low relative abundances of other n-alkanes ranging between C14 and C32–C40 [126–128].

During the ATEX cruise, ALKs highlighted the absence of any odd/even predominance: CPI was 0.83 ± 0.25 (2011) and 0.96 ± 0.08 (2012). These figures are perfectly in agreement with ALKs CPI reported over sea by several authors [41,42,129]. These CPI values support the observation that the measured ALKs were influenced by the sea-to-air emissions, indicating the possibility that a part of the total carbon concentrations in the marine aerosols from the Arctic Ocean could be emitted by the sea. This observation is supported by the evidence when data from ATEX2011 are compared to that measured during ATEX2012 (Figure 13). Particularly, it is evident that, unlike PAHs, ALKs were more abundant during 2012. Again, the air mass back trajectories (2011–2012 in Figures S1 and S2, Supplementary Material) can explain this behavior: during 2012 more air masses travelled over the Arctic Ocean than in 2011 allowing for the capture of much more ALKs from marine origin. Moreover, to support this point, the ALKs in vapor phase were also investigated. Their concentrations ranged from 1 pg m^{-3} to 28.52 ng m^{-3} . Their pattern, presented in Figure 14, is very close to that observed in the particulate phase.

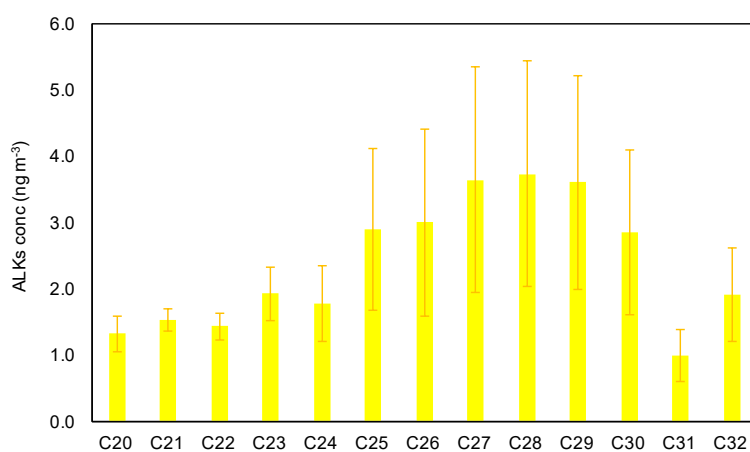


Figure 14. ALKs pattern in gas phase during ATEX2011.

Thus, as done for PAHs, data reported in Figures 13 and 14, were used to calculate the experimental K_p that was then compared with the calculated ones (following the approach of Sangiorgi et al. [69] as described in Section 2.2.4). Results are reported in Figure 15a,b, from which it is evident that the collected samples are spread below the 1:1 line, without any visible linear correlation, and thus, the ALKs phase-partitioning in the particulate phase was underestimated by the dual model. Moreover, if the data are averaged for each ALKs species (Figure 15b), the linear correlation between the experimental and predicted K_p reached poor correlation values ($R^2 = 0.485$) with a slope close to two (1.747) and also with an important negative intercept (-2.764), which again describe the underestimation in the particle phase of the dual model. These results, together with the CPI values, showed that ALKs were emitted from the sea in the particulate phase and support the observation that the total carbon concentrations in the marine aerosols from the Arctic Ocean could be influenced by the sea-to-air emissions of marine OM (Section 3.2) directly in the aerosol phase.

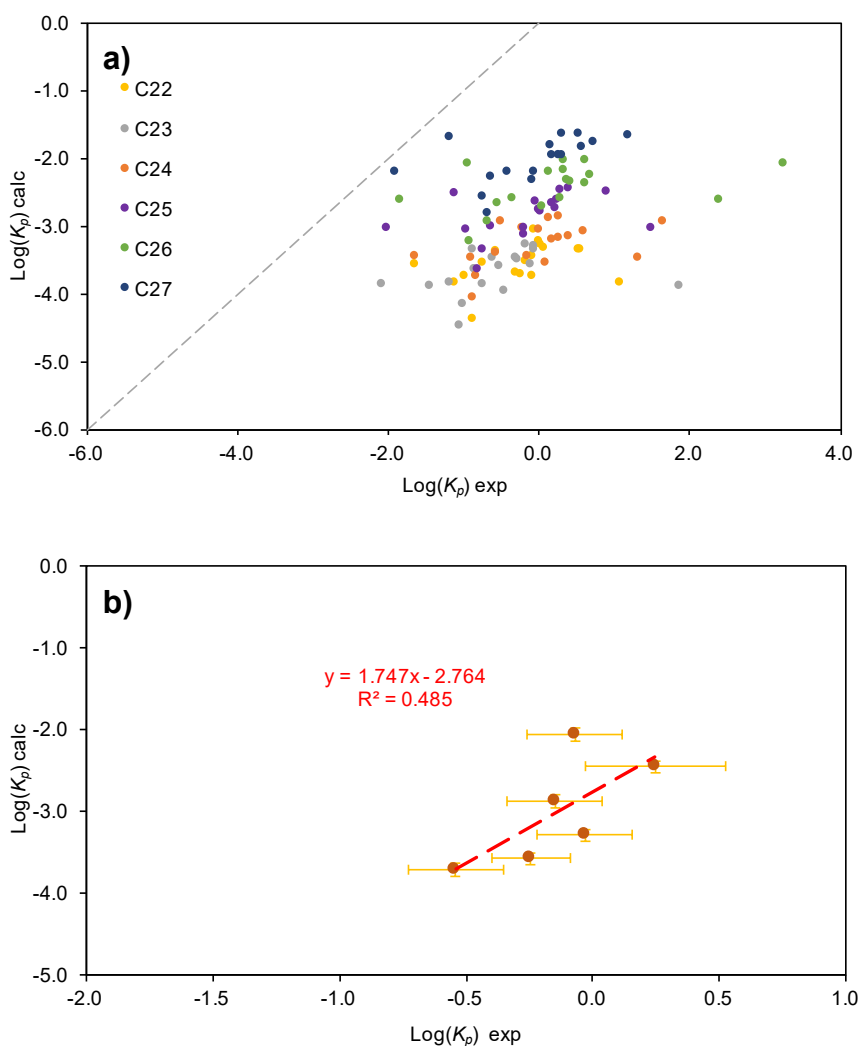


Figure 15. Experimental and predicted K_p for semi-volatile ALKs for each collected sample (a), and averaged for each ALK species (b).

3.4. Element Concentrations

The measured elements were split into three groups: major trace, minor trace, and REEs.

Major trace elements include these metals whose average mass concentrations $> 1 \text{ ng m}^{-3}$ such as Al, Fe, Cu, and Zn, while minor trace elements, such as Cd, Ba, Pb, Ti, V, Cr, Mn, Ni, As, and Mo are considered as those with average concentrations $< 1 \text{ ng m}^{-3}$. REEs showing concentrations higher

than their detection limits in most of the samples are also reported here, namely Y, La, Ce, Pr, Nd, Sm, Eu, Gd, Tb, Dy, Er, Tm, Yb, and Sc.

Figure 16 reports the box plots showing the distribution of concentration levels for the three classes of elements in the aerosol samples collected during the AREX 2011 campaign.

Al and Fe were found to be present at the largest concentrations among trace metals, with an average concentration of 10.85 ± 15.07 and 14.07 ± 22.08 ng m⁻³, respectively, accounting for the 0.23% and 0.30% of the PM total load (assessed by gravimetric determination on the same filters) and for the 1.2% and 1.5%, respectively, of the total metal content, including alkaline and earth-alkaline metals. The two metals are the most abundant in the earth's crust and their linear correlation considering all the samples is high and significant ($R = 0.867$ with 61 samples) shows that crustal input was the dominant source for both of them. In fact, Al, being the most abundant and stable metal in the upper continental crust, is usually taken as reference to assess the extra-crustal source for other metals in atmospheric aerosol. The slope of the Fe versus Al correlation (1.37) marked a very slight enrichment for Fe with respect to earth's average composition yielding an enrichment factor (EF) of 1.44, calculated on the basis of Fe/Al ratio in the upper continental crust (0.95 w/w) [130]; however, given the uncertainty carried along by such ratios and standard deviations of the aerosol measurements here reported (higher than averages), such an enrichment cannot be taken as significant. The Fe/Al ratio ranged between 0.36 and 4.65 with no particular trend during the whole campaign, supporting the main contribution of mineral dust to these two metals with the possible exception of a few days with a larger contribution of Fe with respect to the contribution expected on the basis of earth's composition (on 01, 06–07, 18–19, 24, and 26 July). On these specific days, Fe EF ranged between 3 to 5 and high values (within this data set) of typically anthropogenic metals, such as As, Cr, Ni, and V, can be observed in Figure 17, hinting at a transport of "polluted" air masses as a likely cause for such high Fe/Al ratios. In order to better constrain the kind of anthropogenic source, further elaboration should be carried out since a simple comparison with a marker of fossil fuel source (SO₄²⁻) does not show any clear and significant correlation with Fe EF nor the content of the typical anthropic metals. All the aforementioned statements agreed with the low fraction of nss-sulfates measured during 2011 (Section 3.1.1).

Among the minor trace elements, Ti, V, Cr, Pb, and Mn are present at the highest levels, with averages comprised between 0.19 ± 0.25 ng m⁻³ (for Mn) and 0.94 ± 1.03 ng m⁻³ (for Ti).

Some of these minor trace metals, namely, Ti, Mn, and Zn, show relatively good linear relationships with Al and such a pattern can be explained through crustal inputs being their common dominant source. Particularly strong correlations were found between both Ti and Mn with Al ($R = 0.861$ and 0.847 , respectively). Nevertheless, a clear difference arose between them, since Ti did not show any significant enrichment with respect to earth's composition when Al was taken as a reference, very similarly to Fe; in fact, the slope of Ti versus Al correlation was 0.053, corresponding to an EF of 1.43 (given that the Ti/Al ratio in earth's crust is 0.037 w/w , according to Rudnick and Gao [130]). This supports Ti as a mainly crustal element. The case of Mn is different; although it shows a good correlation with Al, the slope was 0.015, while the Earth's upper crust shows an average Mn/Al ratio of 0.11 [130], indicating that aerosol samples collected here show a depletion of Mn with respect to mean crustal composition. This can be explained by an actually different composition of the crustal inputs supplying Mn to the Arctic region we have studied or by the uncertainties carried along by the average crustal ratios and by the measurements of very low levels of Mn in these samples and this needs further investigation. Zn behaves differently, showing a rather good correlation ($R = 0.679$) and an EF of 108 (Zn/Al ratio in upper crust is 8.2×10^{-4} w/w), which is significantly high and enables to state that Zn present in the samples arose both from mineral dust (no correlation with Al would be found otherwise) and from extra sources, likely together with air masses advected to the Arctic Ocean from lower latitudes.

As concerning REEs, as one can see from Figures 15 and 16, they present average concentration levels ranging between 0.1 and 10 pg m⁻³ (the y-scale in both the figures is expressed as ng m⁻³ to be

compared with the other plots), with Ce, La, Y, and Nd as the most abundant elements in this class. Such values are in agreement with the measurements of REEs in PM₁₀ aerosol collected at Ny-Ålesund, as reported by Giardi et al. [77,131]. They all show a large variability of values, mainly related to the contribution of different crustal sources containing REEs, as shown in previous works [120]. They all correlate quite well with Al (linear correlation coefficients ranging between 0.55 and 0.80) showing that mineral dust is also a major source contribution for these elements. Nevertheless, as shown in previous works [132], they also arose from anthropic activities, such as ship emissions, since they are also present in heavy oil used as fuel for ships. On the basis of Moreno et al. [74], particular La/Ce and La/V ratios can be used to identify the samples characterized by a significant contribution from ship emissions; by taking into account these ratios (La/Ce between 0.6 and 0.8 and La/V lower than 0.1), about the 30% of the samples here analyzed can be related to a relevant contribution of ship emissions. Interestingly, all of them refer to the first part of the cruise (before July 8), involving the ocean areas located south of Spitsbergen, and probably more affected by heavy touristic and commercial ship traffic during the summer period.

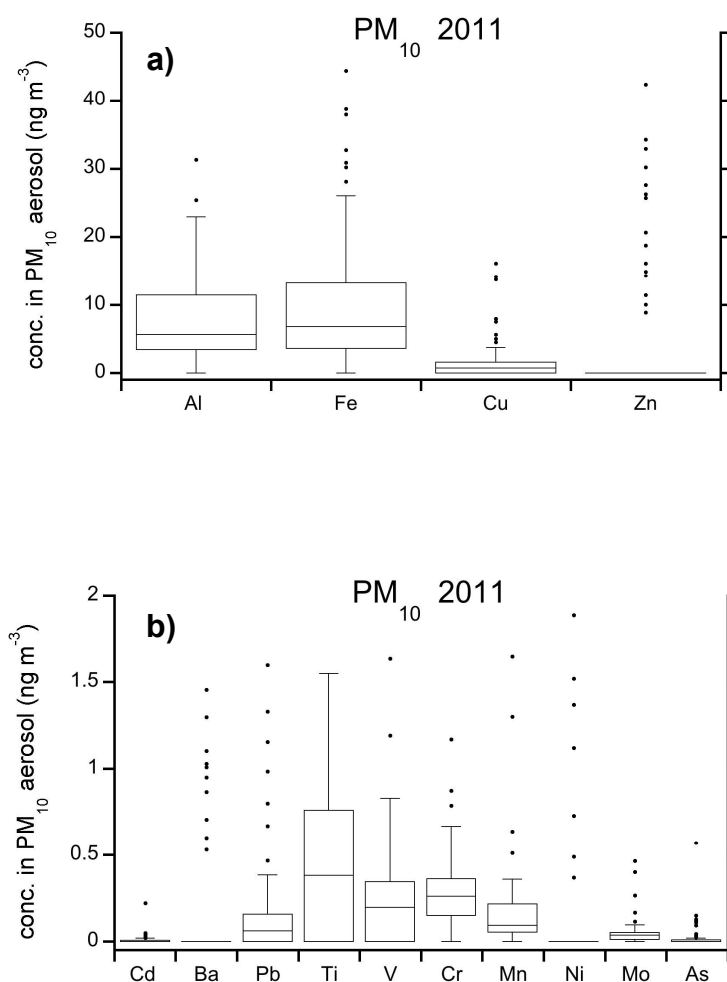


Figure 16. Cont.

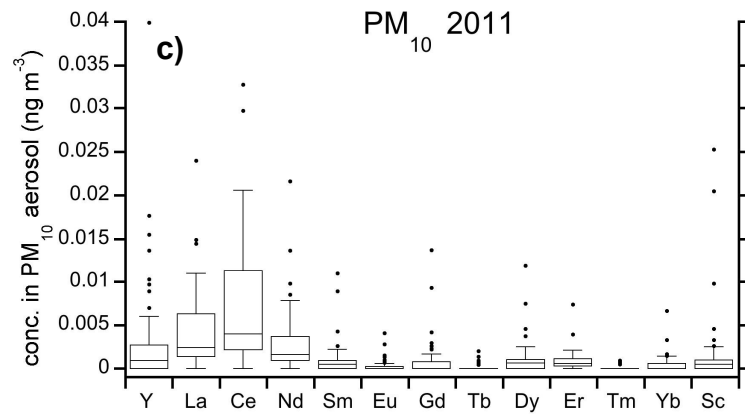


Figure 16. Box plot of trace metal concentrations measured in PM₁₀ aerosol during the AREX 2011 cruise. In order to differentiate the value distribution of all metals, the determined parameters were classified as “major trace” (a), “minor trace” (b), and “REEs” (c).

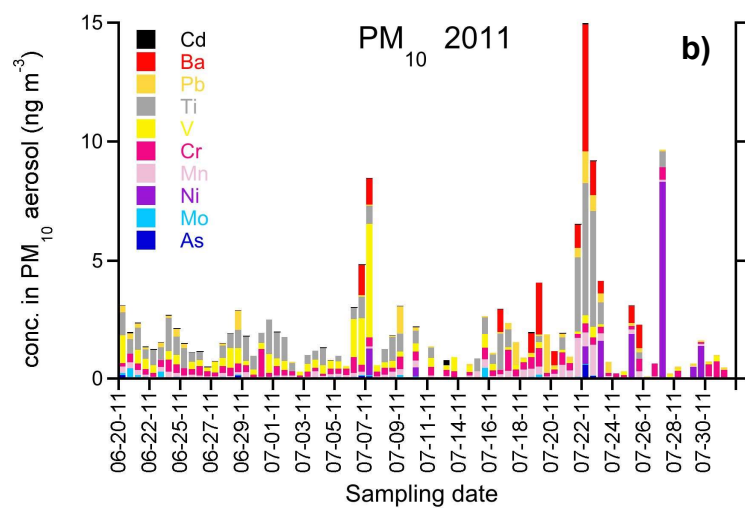
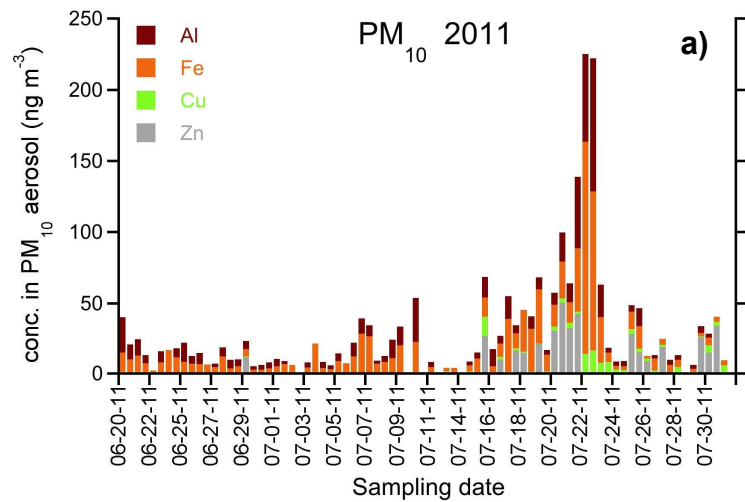


Figure 17. Cont.

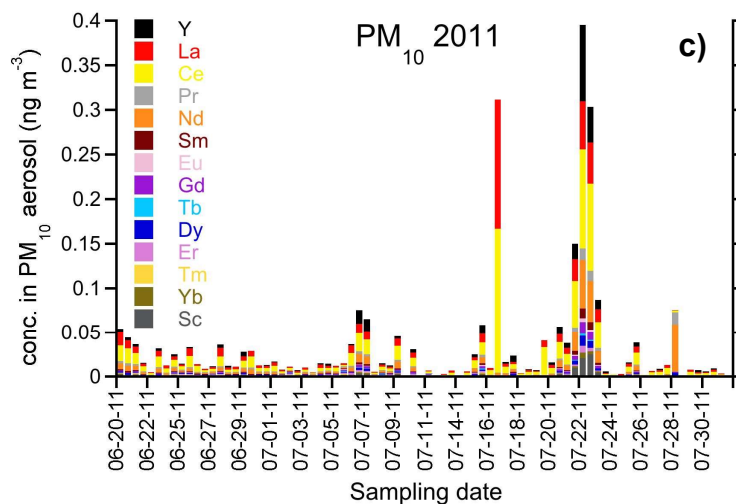


Figure 17. Stack column plots showing the concentration versus time profiles for trace metal concentrations measured in PM_{10} aerosol during the AREX 2011 cruise. In order to differentiate the value distribution of all the metals, the determined parameters were classified as “major trace” (a), “minor trace” (b), and “REEs” (c).

4. Conclusions

The chemical composition of the aerosol over the Arctic Ocean was determined during two years of field campaigns (2011 and 2012) by using a combination of mass spectrometry, ion chromatography, and thermo-optical-transmission techniques enabling us to investigate the water-soluble inorganic and organic compounds, and the carbon content together with PAHs and ALKs behavior, both in gas and particle phase. Moreover, trace elements and rare earth elements were investigated for the first time over the open sea in the Arctic. Samples were collected on board the Polish research vessel *Oceania*, during cruises from Tromsø to Svalbard and from Svalbard to Greenland. At the same time, aerosol samples were also collected at Ny-Ålesund and analyzed for the same chemical species. Results firstly lead to the conclusion that the ionic components accounted for more than 70% of particle mass and more than 90% of inorganic ions originated from sea salt. Only the sulfates exhibited a non-sea-salt origin in large part due to both transport from mid-latitudes and a local secondary origin from phytoplankton activity. The organic matter (OM) accounted for more than 95% of the total carbon, while the remaining 5% was due to long-range transported elemental carbon (EC). The OM aerosol was comparable to that of Cl^- . Important results came out from the comparison with land-based data in Ny-Ålesund: the sea salt concentrations were systematically 7 times higher over the ocean; higher concentrations of OM, ammonium, sulfate, and nitrate were also determined along the cruise than over the land. These results show a significant need to carry out experimental measurements in open seas, similarly to the long-term land-based measurements and intensive observational campaigns (cruise-based) become a complementary source of information concerning the aerosol chemical composition in the Arctic.

Among the organic material, organic ions appeared to be present at significant levels, especially the amines (dimethylamine, trimethylamine, diethylamine) that were found at concentrations of 3.98 ± 1.21 , 1.70 ± 0.82 , and 1.06 ± 0.56 p.p.t.v. (parts per trillion by volume). These values were particularly relevant because they are close to those used in the CLOUD chamber experiments when the ambient nucleation rate in a H_2SO_4 -DMA- H_2O system was simulated, thus stressing again the importance of the detected amines in polar regions. The gas/particle partitioning of organic pollutants (PAHs) or tracer of organic carbon origin (n-alkanes) was evaluated, modelled, and compared with experimental data. Results demonstrated a good equilibrium between particle and gas phase for PAHs; in this respect a south to north increase of the semivolatile fraction was evidenced in keeping with literature data. Instead, n-alkanes phase partitioning (together with the low CPI values) suggested a local marine origin.

Finally, trace elements showed a large variability in concentration and could be classified as major trace elements (Al, Fe, Cu, and Zn) with concentrations $> 1 \text{ ng m}^{-3}$, minor trace elements (Cd, Ba, Pb, Ti, V, Cr, Mn, Ni, As, and Mo) with concentrations $< 1 \text{ ng m}^{-3}$, and REEs elements (Y, La, Ce, Pr, Nd, Sm, Eu, Gd, Tb, Dy, Er, Tm, Yb, and Sc) showing concentrations at pg m^{-3} levels. Specific element ratios highlighted the dominant anthropic contribution for major and minor metals (e.g., Zn, As, Cd, Ni) and the possible signature of ship emissions (La/Ce and La/V)

Supplementary Materials: The following materials are available online at <http://www.mdpi.com/2073-4433/10/2/54/s1>, Figure S1: Five-day air mass back trajectories derived using the HYSPLIT for every AREX2011 TSP sample collected along the cruise. Figure S2: Five-day air mass back trajectories derived using the HYSPLIT for every AREX2012 TSP sample collected along the cruise. Table S1: CAMS output obtained with a 0.125° cell resolution every 3-h following the vessel position (latitude, longitude) and averaging the data accordingly to sampling time and location of each TSP aerosol samples collected along the cruise.

Author Contributions: Conceptualization, L.F., T.Z., E. B. and T.P.; Methodology, G.S., M.G.P.; Software, P.P.; Validation, G.S., L.F., R.T. and S.B.; Formal Analysis, L.F.; Investigation, G.S., M.G.P., C.R., M.C., R.T., S.B., P.M. (Piotr Markuszewski), P.M. (Przemysław Makuch); Resources, T. Z., E.B., R.T., S.B. and T.P.; Data Curation, L.F., G.S., C.R., R.T.; Writing-Original Draft Preparation, L.F.; Writing-Review & Editing, L.F.; Supervision, T.Z., R.T., C.R.; Project Administration, E.B. and T.Z.

Funding: This research received no external funding.

Acknowledgments: This paper is an output of GEMMA center in the framework of Project-MIUR “Dipartimento di Eccellenza 2018-2022”. We acknowledge CAMS project, funded under the Regulation (EU) No 377/2014 of the European Parliament and of the Council of April 3, 2014, establishing the Copernicus Programme (“the Copernicus Regulation”), and operated by ECMWF under an agreement with the European Commission dated November 11, 2014 (“ECMWF Agreement”), for provided data. We kindly acknowledge Prof. Roberto Udisti that, even though retired, gave his contribution allowing us to start this international cooperation and related measurements.

Conflicts of Interest: The authors declare no conflict of interest. The funders had no role in the design of the study; in the collection, analyses, or interpretation of data; in the writing of the manuscript, or in the decision to publish the results.

References

1. IPCC. *Climate Change 2013: The Physical Science Basis*; Cambridge University Press: Cambridge, UK; New York, NY, USA, 2013.
2. Serreze, M.C.; Barrett, A.P.; Stroeve, J.C.; Kindig, D.N.; Holland, M.M. The emergence of surface-based Arctic amplification. *Cryosphere* **2009**, *3*, 11–19. [[CrossRef](#)]
3. Shindell, D.; Faluvegi, G. Climate response to regional radiative forcing during the twentieth century. *Nat. Geosci.* **2009**, *2*, 294–300. [[CrossRef](#)]
4. Bond, T.C.; Doherty, S.J.; Fahey, D.W.; Forster, P.M.; Berntsen, T.; Deangelo, B.J.; Flanner, M.G.; Ghan, S.; Kärcher, B.; Koch, D.; et al. Bounding the role of black carbon in the climate system: A scientific assessment. *J. Geophys. Res.* **2013**, *118*, 1–173. [[CrossRef](#)]
5. Ramanathan, V.; Feng, Y. Air pollution, greenhouse gases and climate change: Global and regional perspectives. *Atmos. Environ.* **2009**, *43*, 37–50. [[CrossRef](#)]
6. Koren, I.; Kaufman, Y.J.; Remer, L.A.; Martins, J.V. Measurements of the effect of amazon smoke on inhibition of cloud formation. *Science* **2004**, *303*, 1342–1345. [[CrossRef](#)] [[PubMed](#)]
7. Koren, I.; Martins, J.V.; Remer, L.A.; Afargan, H. Smoke invigoration versus inhibition of clouds over the amazon. *Science* **2008**, *321*, 946–949. [[CrossRef](#)] [[PubMed](#)]
8. Kaufman, Y.J.; Tanré, D.; Boucher, O. A satellite view of aerosols in the climate system. *Nature* **2002**, *419*, 215–223. [[CrossRef](#)] [[PubMed](#)]
9. Navarro, J.C.A.; Varma, V.; Riipinen, I.; Seland, Ø.; Kirkevåg, A.; Struthers, H.; Iversen, T.; Hansson, H.-C.; Ekman, A.M.L. Amplification of Arctic warming by past air pollution reductions in Europe. *Nat. Geosci.* **2016**. [[CrossRef](#)]
10. Maturilli, M.; Herber, H.; König-Langlo, G. Surface radiation climatology for Ny-Ålesund, Svalbard (78.9° N), basic observations for trend detection. *Theor. Appl. Climatol.* **2015**, *120*, 331–339. [[CrossRef](#)]
11. Isaksen, K.; Nordli, Ø.; FØrland, E.J.; Lupikasza, E.; Eastwood, S.; Niedzwiedz, T. Recent warming on Spitzbergen—Influence of atmospheric circulation and sea ice cover. *J. Geophys. Res. Atmos.* **2016**. [[CrossRef](#)]

12. Ødemark, K.; Dalsøren, S.B.; Samset, B.H.; Berntsen, T.K.; Fuglestad, J.S.; Myhre, G. Short-lived climate forcers from current shipping and petroleum activities in the Arctic. *Atmos. Chem. Phys.* **2012**, *12*, 1979–1993. [[CrossRef](#)]
13. Shindell, D.; Kuylensstierna, J.C.I.; Vignati, E.; Van Dingenen, R.; Amann, M.; Klimont, Z.; Anenberg, S.C.; Müller, N.; Janssens-Maenhout, G.; Raes, F.; et al. Simultaneously mitigating near-term climate change and improving human health and food security. *Science* **2012**, *335*, 183–189. [[CrossRef](#)] [[PubMed](#)]
14. Jacobson, M.Z. Short-term effects of controlling fossil-fuel soot, biofuel soot and gases, and methane on climate, arctic ice, and air pollution health. *J. Geophys. Res.* **2010**, *115*, D14209. [[CrossRef](#)]
15. Quinn, P.K.; Bates, T.S.; Baum, E.; Doubleday, N.; Fiore, M.; Flanner, M.; Fridlind, A.; Garrett, T.J.; Koch, D.; Menon, S.; et al. Short-lived pollutants in the Arctic: Their climate impact and possible mitigation strategies. *Atmos. Chem. Phys.* **2008**, *8*, 1723–1735. [[CrossRef](#)]
16. Sand, M.; Berntsen, T.K.; Von Salzen, K.; Flanner, M.G.; Lagner, J.; Victor, D.G. Response of Arctic temperature to changes in emissions of short-lived climate forcers. *Nat. Clim. Chang.* **2015**. [[CrossRef](#)]
17. Serreze, M.C.; Barry, R.G. Processes and impacts of Arctic amplification: A research synthesis. *Glob. Planet. Chang.* **2011**, *77*, 85–96. [[CrossRef](#)]
18. Stohl, A.; Klimont, Z.; Eckhardt, S.; Kupiainen, K.; Shevchenko, V.P.; Kopeikin, V.M.; Novigatsky, A.N. Black carbon in the Arctic: The underestimated role of gas flaring and residential combustion emissions. *Atmos. Chem. Phys.* **2013**. [[CrossRef](#)]
19. Sand, M.; Berntsen, T.K.; Kay, J.E.; Lamarque, J.F.; Seland, Ø.; Kirkevåg, A. The Arctic response to remote and local forcing of black carbon. *Atmos. Chem. Phys.* **2013**, *13*, 211–224. [[CrossRef](#)]
20. Screen, J.A.; Simmonds, I. The central role of diminishing sea ice in recent Arctic temperature amplification. *Nature* **2010**, *464*, 1334–1337. [[CrossRef](#)]
21. Screen, J.A.; Simmonds, I. Increasing fall-winter energy loss from the Arctic Ocean and its role in Arctic temperature amplification. *Geophys. Res. Lett.* **2010**, *37*, L16707. [[CrossRef](#)]
22. Dall’Osto, M.; Beddows, D.C.S.; Tunved, P.; Krejci, R.; Ström, J.; Hansson, H.C.; Yoon, Y.J.; Park, K.T.; Becagli, S.; Udisti, R.; et al. Arctic sea ice melt leads to atmospheric new particle formation. *Sci. REP-UK* **2017**, *7*, 3318. [[CrossRef](#)] [[PubMed](#)]
23. Francis, J.A.; Hunter, E. New insight into the disappearing Arctic sea ice. *EOS Trans. Am. Geophys. Union* **2006**, *87*, 509–511. [[CrossRef](#)]
24. Ferrero, L.; Mocnik, G.; Ferrini, B.S.; Perrone, M.G.; Sangiorgi, G.; Bolzacchini, E. Vertical profiles of aerosol absorption coefficient from micro-Aethalometer data and Mie calculation over Milan. *Sci. Total Environ.* **2011**, *409*, 2824–2837. [[CrossRef](#)] [[PubMed](#)]
25. Ferrero, L.; Castelli, M.; Ferrini, B.S.; Moscatelli, M.; Perrone, M.G.; Sangiorgi, G.; D’Angelo, L.; Rovelli, G.; Moroni, B.; Scardazza, F.; et al. Impact of black carbon aerosol over Italian basin valleys: High-resolution measurements along vertical profiles, radiative forcing and heating rate. *Atmos. Chem. Phys.* **2014**, *14*, 9641–9664. [[CrossRef](#)]
26. Ferrero, L.; D’Angelo, L.; Rovelli, G.; Sangiorgi, G.; Perrone, M.G.; Moscatelli, M.; Casati, M.; Rozzoni, V.; Bolzacchini, E. Determination of aerosol deliquescence and crystallization relative humidity for energy saving in free-cooled data centers. *Environ. Sci. Technol.* **2015**. [[CrossRef](#)]
27. Collaud Coen, M.; Andrews, E.; Asmi, A.; Baltensperger, U.; Bukowiecki, N.; Day, D.; Fiebig, M.; Fjaeraa, A.M.; Flenje, H.; Hyvarinen, A.; et al. Aerosol decadal trends—Part 1: In-situ optical measurements at GAW and IMPROVE stations. *Atmos. Chem. Phys.* **2013**. [[CrossRef](#)]
28. Hirdman, D.; Sodemann, H.; Eckhardt, S.; Burkhardt, J.F.; Jefferson, A.; Mefford, T.; Quinn, P.K.; Sharma, S.; Strom, J.; Stohl, A. Source identification of short-lived air pollutants in the Arctic using statistical analysis of measurements data and particle dispersion model output. *Atmos. Chem. Phys.* **2010**, *10*, 669–693. [[CrossRef](#)]
29. Flanner, M.G. Arctic climate sensitivity to local black carbon. *J. Geophys. Res. Atmos.* **2013**, *118*, 1840–1851. [[CrossRef](#)]
30. Eckhardt, S.; Hermansen, O.; Grythe, H.; Fiebig, M.; Stebel, K.; Cassiani, M.; Baecklund, A.; Stohl, A. The influence of cruise ship emissions on air pollution in Svalbard—A harbinger of a more polluted Arctic? *Atmos. Chem. Phys.* **2013**, *13*, 8401–8409. [[CrossRef](#)]
31. Stohl, A. Characteristics of atmospheric transport into the Arctic troposphere. *J. Geophys. Res. Atmos.* **2006**, *111*, D11306. [[CrossRef](#)]

32. Ferrero, L.; Cappelletti, D.; Busetto, M.; Mazzola, M.; Lupi, A.; Lanconelli, C.; Becagli, S.; Traversi, R.; Caiazzo, L.; Giardi, F.; et al. Vertical profiles of aerosol and black carbon in the Arctic: A seasonal phenomenology along 2 years (2011–2012) of field campaigns. *Atmos. Chem. Phys.* **2016**, *16*, 12601–12629. [[CrossRef](#)]
33. Kupiszewski, P.; Leck, C.; Tjernström, M.; Sjogren, S.; Sedlar, J.; Graus, M.; Müller, M.; Brooks, B.; Swietlicki, E.; Norris, S.; et al. Vertical profiling of aerosol particles and trace gases over the central Arctic Ocean during summer. *Atmos. Chem. Phys.* **2013**, *13*, 12405–12431. [[CrossRef](#)]
34. Tunved, P.; Ström, J.; Krejci, R. Arctic aerosol life cycle: Linking aerosol size distributions observed between 2000 and 2010 with air mass transport and precipitation at Zeppelin station, Ny-Ålesund, Svalbard. *Atmos. Chem. Phys.* **2013**, *13*, 3643–3660. [[CrossRef](#)]
35. Udisti, R.; Bazzano, A.; Becagli, S.; Bolzacchini, E.; Caiazzo, L.; Cappelletti, D.; Ferrero, L.; Frosini, D.; Giardi, F.; Grotti, M.; et al. Sulfate source apportionment in the Ny Ålesund (Svalbard Islands) Arctic aerosol. *Rend. Lincei* **2016**. [[CrossRef](#)]
36. Zielinski, T.; Petelski, T.; Strzałkowska, A.; Pakszys, P.; Makuch, P. Impact of wild forest fires in Eastern Europe on aerosol composition and particle optical properties. *Oceanologia* **2016**, *58*, 13–24. [[CrossRef](#)]
37. Pakszys, P.; Zieliński, T.; Markowicz, K.; Petelski, T.; Makuch, P.; Lisok, J.; Chiliński, M.; Rozwadowska, A.; Ritter, C.; Neuber, R.; et al. Annual changes of aerosol optical depth and Ångström exponent over Spitsbergen. *Impact Clim. Change. Mar. Environ.* **2015**, *1*, 23–36. [[CrossRef](#)]
38. Corbett, J.J.; Lack, D.A.; Winebrake, J.J.; Harder, S.; Silberman, J.A.; Gold, M. Arctic shipping emissions inventories and future scenarios. *Atmos. Chem. Phys.* **2010**, *10*, 9689–9704. [[CrossRef](#)]
39. Riccobono, F.; Schobesberger, S.; Scott, C.E.; Dommen, J.; Ortega, I.K.; Rondo, L.; Almeida, J.; Amorim, A.; Bianchi, F.; Breitenlechner, M.; et al. Oxidation Products of Biogenic Emissions Contribute to Nucleation of Atmospheric Particles. *Science* **2014**, *344*, 717–721. [[CrossRef](#)]
40. Almeida, J.; Schobesberger, S.; Kürten, A.; Ortega, I.K.; Kupiainen-Maättä, O.; Praplan, A.P.; et al. Molecular understanding of sulphuric acid–amine particle nucleation in the atmosphere. *Nature* **2013**, *502*, 359–363. [[CrossRef](#)]
41. Marty, J.C.; Saliot, A. Hydrocarbons (normal alkanes) in the surface microlayer of seawater. *Deep Sea Res.* **1976**, *23*, 863–873. [[CrossRef](#)]
42. Stortini, A.M.; Martellini, T.; Del Bubba, M.; Lepri, L.; Capodaglio, G.; Cincinelli, A. n-Alkanes, PAHs and surfactants in the sea surface microlayer and sea water samples of the Gerlache Inlet sea (Antarctica). *Microchem. J.* **2009**, *92*, 37–43. [[CrossRef](#)]
43. Hansen, A.M.K.; Kristensen, K.; Nguyen, Q.T.; Zare, A.; Cozzi, F.; Nøjgaard, J.K.; Skov, H.; Brandt, J.; Christensen, J.H.; Strom, J.; et al. Organosulfates and organic acids in Arctic aerosols: Speciation, annual variation and concentration levels. *Atmos. Chem. Phys.* **2014**. [[CrossRef](#)]
44. Martin, S.T. Phase Transitions of Aqueous Atmospheric Particles. *Chem. Rev.* **2000**, *100*, 3403–3453. [[CrossRef](#)] [[PubMed](#)]
45. Kawamura, K.; Kasukabe, H.; Barrie, L.A. Source and reaction pathways of dicarboxylic acids, ketoacids and dicarbonyls in arctic aerosols: One year of observations. *Atmos. Environ.* **1996**, *30*, 1709–1722. [[CrossRef](#)]
46. Ervens, B.; Feingold, G.; Frost, G.J.; Kreidenweis, S.M. A modeling study of aqueous production of dicarboxylic acids: 1. Chemical pathways and speciated organic mass production. *J. Geophys. Res.* **2004**, *109*, D15205. [[CrossRef](#)]
47. Kawamura, K.; Kaplan, I.R. Motor exhaust emissions as a primary source for dicarboxylic acids in Los Angeles ambient air. *Environ. Sci. Technol.* **1987**, *21*, 105–110. [[CrossRef](#)]
48. Legrand, M.; De Angelis, M. Light carboxylic acids in Greenland ice: A record of past forest fires and vegetation emissions from the boreal zone. *J. Geophys. Res.* **1996**, *101*, 4129–4145. [[CrossRef](#)]
49. Kundu, S.; Kawamura, K.; Andreae, T.W.; Hoffer, A.; Andreae, M.O. Molecular distributions of dicarboxylic acids, ketocarboxylic acids and alpha-dicarbonyls in biomass burning aerosols: Implications for photochemical production and degradation in smoke layers. *Atmos. Chem. Phys.* **2010**, *10*, 2209–2225. [[CrossRef](#)]
50. Kawamura, K.; Narukawa, M.; Li, S.M.; Barrie, L.A. Size distributions of dicarboxylic acids and inorganic ions in atmospheric aerosols collected during polar sunrise in the Canadian high Arctic. *J. Geophys. Res. Atmos.* **2012**, *112*, D10307. [[CrossRef](#)]

51. Kawamura, K.; Ono, K.; Tachibana, E.; Charrière, B.; Sempéré, R. Distributions of low molecular weight dicarboxylic acids, ketoacids and α -dicarbonyls in the marine aerosols collected over the Arctic Ocean during late summer. *Biogeosciences* **2012**, *9*, 4725–4737. [[CrossRef](#)]
52. Narukawa, M.; Kawamura, K.; Li, S.M.; Bottenheim, J.W. Dicarboxylic acids in the Arctic aerosols and snowpacks collected during ALERT 2000. *Atmos. Environ.* **2002**, *36*, 2491–2499. [[CrossRef](#)]
53. Narukawa, M.; Kawamura, K.; Anlauf, K.G.; Barrie, L.A. Fine and coarse modes of dicarboxylic acids in the Arctic aerosols collected during the Polar Sunrise Experiment 1997. *J. Geophys. Res. Atmos.* **2003**, *108*, 4575. [[CrossRef](#)]
54. Chung, C.E.; Ramanathan, V.; Decremer, D. Observationally constrained estimates of carbonaceous aerosol radiative forcing. *Proc. Natl. Acad. Sci. USA* **2012**, *109*, 11624–11629. [[CrossRef](#)]
55. Shamjad, P.M.; Tripathi, S.N.; Pathak, R.; Hallquist, M.; Arola, A.; Bergin, M.H. Contribution of Brown Carbon to Direct Radiative Forcing over the Indo-Gangetic Plain. *Environ. Sci. Technol.* **2015**, *49*, 10474–10481. [[CrossRef](#)] [[PubMed](#)]
56. Ferrero, L.; Močnik, G.; Cogliati, S.; Gregorič, A.; Colombo, R.; Bolzacchini, E. Heating rate of light absorbing aerosols: Time-resolved measurements and source-identification. *Environ. Sci. Technol.* **2018**, *52*, 3546–3555. [[CrossRef](#)] [[PubMed](#)]
57. Laskin, A.; Laskin, J.; Nizkorodov, S.A. Chemistry of Atmospheric Brown Carbon. *Chem. Rev.* **2015**, *115*, 4335–4382. [[CrossRef](#)] [[PubMed](#)]
58. Halsall, C.J.; Barrie, L.A.; Fellin, P.; Muir, D.C.G.; Billeck, B.N.; Lockhart, L.; Rovinsky, F.Y.; Kononov, E.Y.; Pastukhov, B. Spatial and Temporal Variation of Polycyclic Aromatic Hydrocarbons in the Arctic Atmosphere. *Environ. Sci. Technol.* **1997**, *31*, 3593–3599. [[CrossRef](#)]
59. Bohlin-Nizzetto, P.; Aas, W.; Warner, N. *Monitoring of Environmental Contaminants in Air and Precipitation 2017*; M-1062; NILU-Norwegian Institute for Air Research: Oslo, Norway, 2017.
60. Bidleman, T.F.; Billings, W.N.; Foreman, W.T. Vapor–particle partitioning of semivolatile organic compounds: Estimates from field collections. *Environ. Sci. Technol.* **1986**, *20*, 1038–1043. [[CrossRef](#)]
61. Tasdemir, Y.; Esen, F. Urban air PAHs: Concentrations, temporal changes and gas/particle partitioning at a traffic site in Turkey. *Atmos. Res.* **2007**, *84*, 1–12. [[CrossRef](#)]
62. Vardar, N.; Tasdemir, Y.; Odabasi, M.; Noll, K.E. Characterization of atmospheric concentrations and partitioning of PAHs in the Chicago atmosphere. *Sci. Total. Environ.* **2004**, *327*, 163–174. [[CrossRef](#)]
63. Daisey, J.M.; McCaffrey, R.J.; Gallagher, R.A. Polycyclic aromatic hydrocarbons and total extractable particulate organic matter in the Arctic Aerosol. *Atmos. Environ.* **1981**, *15*, 1353–1363. [[CrossRef](#)]
64. Ma, Y.G.; Lei, Y.D.; Xiao, H.; Wania, F.; Wang, W.H. Critical review and recommended values for the physical–chemical property data of 15 polycyclic aromatic hydrocarbons at 25 °C. *J. Chem. Eng. Data* **2009**, *55*, 819–825. [[CrossRef](#)]
65. Callén, M.S.; de la Cruz, M.T.; López, J.M.; Murillo, R.; Navarro, M.V.; Mastral, A.M. Some inferences on the mechanism of atmospheric gas/ particle partitioning of polycyclic aromatic hydrocarbons (PAH) at Zaragoza (Spain). *Chemosphere* **2008**, *73*, 1357–1365.
66. Demircioglu, E.; Sofuoglu, A.; Odabasi, M. Atmospheric concentrations and phase partitioning of polycyclic aromatic hydrocarbons in Izmir, Turkey. *CLEAN—Soil Air Water* **2011**, *39*, 319–327. [[CrossRef](#)]
67. Fernández, P.; Grimalt, J.O.; Vilanova, R.M. Atmospheric gas–particle partitioning of polycyclic aromatic hydrocarbons in high mountain regions of Europe. *Environ. Sci. Technol.* **2002**, *36*, 1162–1168. [[CrossRef](#)]
68. Van Drooge, B.L.; Fernández, P.; Grimalt, J.O.; Stuchlík, E.; Torres García, C.J.; Cuevas, E. Atmospheric polycyclic aromatic hydrocarbons in remote European and Atlantic sites located above the boundary mixing layer. *Environ. Sci. Pollut. Res.* **2010**, *17*, 1207–1216. [[CrossRef](#)] [[PubMed](#)]
69. Sangiorgi, G.; Ferrero, L.; Perrone, M.; Papa, E.; Bolzacchini, E. Semivolatile PAH and n-alkane gas/particle partitioning using the dual model: Up-to-date coefficients and comparison with experimental data. *Environ. Sci. Pollut. Res.* **2014**, *21*, 10163–10173. [[CrossRef](#)] [[PubMed](#)]
70. Wang, W.; Simonich, S.L.M.; Wang, W.; Giri, B.; Zhao, J.; Xue, M.; Cao, J.; Lu, X.; Tao, S. Atmospheric polycyclic aromatic hydrocarbon concentrations and gas/particle partitioning at background, rural village and urban sites in the North China Plain. *Atmos. Res.* **2011**, *99*, 197–206. [[CrossRef](#)]
71. Maenhaut, W.; Zoller, W.H.; Duce, R.A.; Hoffman, G.L. Concentration and size distribution of particulate trace elements in the south polar atmosphere. *J. Geophys. Res.* **1979**, *84*, 2421–2431. [[CrossRef](#)]

72. Maenhaut, W.; Cornille, P.; Pacyna, J.M.; Vitols, V. Trace element composition and origin of the atmospheric aerosol in the Norwegian Arctic. *Atmos. Environ.* **1989**, *23*, 2551–2569. [[CrossRef](#)]
73. Ferrat, M.; Weiss, D.J.; Strekopytov, S.; Donga, S.; Chen, H.; Najorka, J.; Sunc, Y.; Gupta, S.; Tada, R.; Sinha, R. Improved provenance tracing of Asian dust sources using rare earth elements and selected trace elements for palaeomonsoon studies on the eastern Tibetan Plateau. *Geochim. Cosmochim. Acta* **2011**, *75*, 6374–6399. [[CrossRef](#)]
74. Moreno, T.; Querol, X.; Castillo, S.; Alastuey, A.; Cuevas, E.; Herrmann, L.; Mounkaila, M.; Elvira, J.; Gibbons, W. Geochemical variations in aeolian mineral particles from the Sahara—Sahel Dust Corridor. *Chemosphere* **2006**, *65*, 261–270. [[CrossRef](#)] [[PubMed](#)]
75. Turetta, C.; Zangrando, R.; Barbaro, E.; Gabrieli, J.; Scalabrin, E.; Zennaro, P.; Gambaro, A.; Toscano, G.; Barbante, C. Water-soluble trace, rare earth elements and organic compounds in Arctic aerosol. *Rend. Lincei* **2016**, *27*, 95–103. [[CrossRef](#)]
76. Singh, D.K.; Kawamura, K.; Yanase, A.; Barrie, L.A. Distributions of Polycyclic Aromatic Hydrocarbons, Aromatic Ketones, Carboxylic Acids, and Trace Metals in Arctic Aerosols: Long-Range Atmospheric Transport, Photochemical Degradation/ Production at Polar Sunrise. *Environ. Sci. Technol.* **2017**, *51*, 8992–9004. [[CrossRef](#)] [[PubMed](#)]
77. Giardi, F.; Traversi, R.; Becagli, S.; Severi, M.; Caiazzo, L.; Ancillotti, C.; Udisti, R. Determination of Rare Earth Elements in multi-year high-resolution Arctic aerosol record by double focusing Inductively Coupled Plasma Mass Spectrometry with desolvation nebulizer inlet system. *Sci. Tot. Environ.* **2018**, *613–614*, 1284–1294. [[CrossRef](#)]
78. Eleftheriadis, K.; Vratolis, S.; Nyeki, S. Aerosol black carbon in the European Arctic: Measurements at Zeppelin station, Ny-Ålesund, Svalbard from 1998–2007. *Geophys. Res. Lett.* **2009**, *36*. [[CrossRef](#)]
79. Ström, J.; Engvall, A.C.; Delbart, F.; Krejci, R.; Treffeisen, R. On small particles in the Arctic summer boundary layer: Observations at two different heights near Ny-Ålesund, Svalbard. *Tellus B* **2009**, *61*, 473–482. [[CrossRef](#)]
80. Vihma, T.; Kilpelainen, T.; Manninen, M.; Sjoblom, A.; Jakobson, E.; Palo, T.; Jaagus, J.; Maturilli, M. Characteristics of Temperature and Humidity Inversions and Low-Level Jets over Svalbard Fjords in Spring. *Adv. Meteorol.* **2011**, *2011*. [[CrossRef](#)]
81. Gustafson, K.E.; Dickhut, R.M. Distribution of polycyclic aromatic hydrocarbons in southern Chesapeake Bay surface water: Evaluation of three methods for determining freely dissolved water concentrations. *Environ. Toxicol. Chem.* **1997**, *16*, 452–461. [[CrossRef](#)]
82. Owoade, O.K.; Olise, F.S.; Obioh, I.B.; Olaniyi, H.B.; Bolzacchini, E.; Ferrero, L.; Perrone, G. PM10 sampler deposited air particulates: Ascertaining uniformity of sample on filter through rotated exposure to radiation. *Nucl. Instrum. Meth. A* **2006**, *564*, 315–318. [[CrossRef](#)]
83. Polissar, A.V.; Hopke, P.K.; Paatero, P.; Malm, W.C.; Sisler, J.F. Atmospheric aerosol over Alaska 2. Elemental composition and sources. *J. Geophys. Res.* **1998**, *103*, 19045–19057. [[CrossRef](#)]
84. Lammel, G.; Klanova, J.; Ilic, P.; Kohoutek, J.; Gasic, B.; Kovacic, I.; Skrdlikova, L. Polycyclic aromatic hydrocarbons in air on small spatial and temporal scales—II. Mass size distributions and gas-particle partitioning. *Atmos. Environ.* **2010**, *44*, 5022–5027. [[CrossRef](#)]
85. Lohmann, R.; Lammel, G. Adsorptive and Absorptive Contributions to the Gas-Particle Partitioning of Polycyclic Aromatic Hydrocarbons: State of Knowledge and Recommended Parametrization for Modeling. *Environ. Sci. Technol.* **2004**, *38*, 3793–3803. [[CrossRef](#)] [[PubMed](#)]
86. Dachs, J.; Eisenreich, S.J. Adsorption onto aerosol soot carbon dominates gas-particle partitioning of polycyclic aromatic hydrocarbons. *Environ. Sci. Technol.* **2000**, *34*, 3690–3697. [[CrossRef](#)]
87. Kalberer, M.; Paulsen, D.; Sax, M.; Steinbacher, M.; Dommen, J.; Prevot, A.S.H.; Fisseha, R.; Weingartner, E.; Frankevich, V.; Zenobi, R.; et al. Identification of polymers as major components of atmospheric organic aerosols. *Science* **2004**, *303*, 1659–1662. [[CrossRef](#)]
88. Götz, C.W.; Scheringer, M.; MacLeod, M.; Roth, C.M.; Hungerbühler, K. Alternative approaches for modeling gas-particle partitioning of semivolatile organic chemicals: Model development and comparison. *Environ. Sci. Technol.* **2007**, *41*, 1272–1278. [[CrossRef](#)] [[PubMed](#)]
89. Van Noort, P.C.M. A thermodynamics-based estimation model for adsorption of organic compounds by carbonaceous materials in environmental sorbents. *Environ. Toxicol. Chem.* **2003**, *22*, 1179–1188. [[CrossRef](#)] [[PubMed](#)]

90. Gaga, E.O.; Ari, A. Gas–particle partitioning of polycyclic aromatic hydrocarbons (PAHs) in an urban traffic site in Eskisehir, Turkey. *Atmos. Res.* **2011**, *99*, 207–216. [[CrossRef](#)]
91. Birch, M.E. Occupational Monitoring of Particulate Diesel Exhaust by NIOSH Method 5040. *Appl. Occup. Environ. Hyg.* **2002**, *17*, 400–405. [[CrossRef](#)]
92. Inness, A.; Baier, F.; Benedetti, A.; Bouarar, I.; Chabrilat, S.; Clark, H.; Clerbaux, C.; Coheur, P.; Engelen, R.J.; Errera, Q.; et al. The MACC reanalysis: An 8 yr data set of atmospheric composition. *Atmos. Chem. Phys.* **2013**, *13*, 4073–4109. [[CrossRef](#)]
93. Morcrette, J.J.; Boucher, O.; Jones, L.; Salmond, D.; Bechtold, P.; Beljaars, A.; Benedetti, A.; Bonet, A.; Kaiser, J.; Razingerg, M.; et al. Aerosol analysis and forecast in the ECMWF Integrated Forecast System. Part I: Forward modelling. *J. Geophys. Res.* **2009**, *114D*, D06206. [[CrossRef](#)]
94. Reddy, M.S.; Boucher, O.; Bellouin, N.; Schulz, M.; Balkanski, Y.; Dufresne, J.L.; Pham, M. Estimates of global multi-component aerosol optical depth and direct radiative perturbation in the Laboratoire de Météorologie Dynamique general circulation model. *J. Geophys. Res.* **2005**, *110*, D10S16. [[CrossRef](#)]
95. Wallace, J.M.; Hobbs, P.V. *Atmospheric Science an Introductory Survey*, 2nd ed.; University of Washington: Seattle, WA, USA, 2006.
96. Bates, T.S.; Quinn, P.K.; Coffman, D.J.; Johnson, J.E.; Miller, T.L.; Covert, D.S.; Wiedensohler, A.; Leinert, S.; Nowak, A.; Neusüss, C. Regional physical and chemical properties of the marine boundary layer aerosol across the Atlantic during Aerosols: An overview. *J. Geophys. Res. Atmos.* **2001**, *106*, 20767–20782. [[CrossRef](#)]
97. Pakkanen, T.A.; Kerminen, V.M.; Hillamo, R.E.; Mäkinen, M.; Mäkelä, T.; Virkkula, A. Distribution of nitrate over sea-salt and soil derived particles implications from a field study. *J. Atmos. Chem.* **1996**, *24*, 189–205. [[CrossRef](#)]
98. Virkkula, A.; Teinilä, K.; Hillamo, R.; Kerminen, V.M.; Saarikoski, S.; Aurela, M.; Koponen, I.K.; Kulmala, M. Chemical size distributions of boundary layer aerosol over the Atlantic Ocean and at an Antarctic site. *J. Geophys. Res.* **2006**, *111*, D05306. [[CrossRef](#)]
99. Mihalopoulos, N.; Stephanou, E.; Kanakidou, M.; Pilitsidis, S.; Bousquet, P. Tropospheric aerosol ionic composition in the Eastern Mediterranean region. *Tellus B* **1997**, *49*, 314–326. [[CrossRef](#)]
100. Pilson, M.E.Q. *An Introduction to the Chemistry of the Sea*, 2nd ed.; Cambridge University Press: Cambridge, UK, 2013.
101. Millero, F.J. *Chemical Oceanography*, 4th ed.; Taylor & Francis Group: Abingdon, UK, 2013.
102. Xu, G.; Gao, Y.; Lin, Q.; Li, W.; Chen, L. Characteristics of water-soluble inorganic and organic ions in aerosols over the Southern Ocean and coastal East Antarctica during austral summer. *J. Geophys. Res. Atmos.* **2013**, *118*, 303–318. [[CrossRef](#)]
103. Moroni, B.; Becagli, S.; Bolzacchini, E.; Busetto, M.; Cappelletti, D.; Crocchianti, S.; Ferrero, L.; Frosini, D.; Lanconelli, C.; Lupi, A.; et al. Vertical Profiles and Chemical Properties of Aerosol Particles upon Ny-Ålesund (Svalbard Islands). *Adv. Meteorol.* **2015**, *292081*, 1–11. [[CrossRef](#)]
104. Moroni, B.; Arnalds, O.; Dagsson-Waldhauserová, P.; Crocchianti, S.; Vivani, R.; Cappelletti, D. Mineralogical and Chemical Records of Icelandic Dust Sources Upon Ny-Ålesund (Svalbard Islands). *Front. Earth Sci.* **2018**, *6*. [[CrossRef](#)]
105. Berresheim, H.; Eisele, F.L. Sulfur chemistry in the Antarctic troposphere experiment: An overview of project SCATE. *J. Geophys. Res.* **1998**, *103*, 1619–1627. [[CrossRef](#)]
106. O’Dowd, C.D.; De Leeuw, G. Marine aerosol production: A review of the current knowledge. *Philos. Trans. R. Soc. A* **2007**, *365*, 1753–1774. [[CrossRef](#)]
107. Massling, A.; Nielsen, I.E.; Kristensen, D.; Christensen, J.H.; Sorensen, L.L.; Jensen, B.; Nguyen, Q.T.; Nojgaard, J.K.; Glasius, M.; Skov, H. Atmospheric black carbon and sulfate concentration in Northeast Greenland. *Atmos. Chem. Phys.* **2015**, *15*, 9681–9692. [[CrossRef](#)]
108. Minikin, A.; Legrand, M.; Hall, J.; Wagenbach, D.; Kleefeld, C.; Wolff, E.; Pasteur, E.C.; Ducroz, F. Sulfur-containing species (sulfate and methanesulfonate) in coastal Antarctic aerosol and precipitation. *J. Geophys. Res.* **1998**, *103*, 975–990. [[CrossRef](#)]
109. Legrand, M.; Ducroz, F.; Wagenbach, D.; Mulvaney, R.; Hall, J. Ammonium in coastal Antarctic aerosol and snow: Role of polar ocean and penguin emissions. *J. Geophys. Res.* **1998**, *103*, 11043–11056. [[CrossRef](#)]
110. Blackall, T.D.; Wilson, L.J.; Theobald, M.R.; Milford, C.; Nemitz, E.; Bull, J.; Bacon, P.J.; Hamer, K.C.; Wanless, S.; Sutton, M.A. Ammonia emissions from seabird colonies. *Geophys. Res. Lett.* **2007**, *34*, L10801. [[CrossRef](#)]

111. Riddick, S.N.; Dragosits, U.; Blackall, T.D.; Daunt, F.; Wanless, S.; Sutton, M.A. The global distribution of ammonia emissions from seabird colonies. *Atmos. Environ.* **2012**, *55*, 319–327. [[CrossRef](#)]
112. Liss, P.S.; Galloway, J.N. *Air-sea Exchange of Sulphur and Nitrogen and Their Interaction in the Marine Atmosphere, in Interactions of C, N, P and S Biogeochemical Cycles and Global Change*; Wollast, R., Mackenzie, F.T., Chou, L., Eds.; Springer: Berlin/Heidelberg, Germany, 1993; Volume 4, pp. 259–281.
113. Jickells, T.D.; Kelly, S.D.; Baker, A.R.; Biswas, K.; Dennis, P.F.; Spokes, L.J.; Witt, M.; Yeatman, S.G. Isotopic evidence for a marine ammonia source. *Geophys. Res. Lett.* **2003**, *30*, 1374. [[CrossRef](#)]
114. Kawamura, K.; Ikushima, K. Seasonal changes in the distribution of dicarboxylic acids in the urban atmosphere. *Environ. Sci. Technol.* **1993**, *27*, 2227–2235. [[CrossRef](#)]
115. Kirkby, J.; Curtius, J.; Almeida, J.; Dunne, E.; Duplissy, J.; Ehrhart, S.; Franchin, A.; Gagné, S.; Ickes, L.; Kürten, A.; et al. Role of sulphuric acid, ammonia and galactic cosmic rays in atmospheric aerosol nucleation. *Nature* **2011**, *476*, 429–433. [[CrossRef](#)] [[PubMed](#)]
116. Reddington, C.L.; Carslaw, K.S.; Spracklen, D.V.; Frontoso, M.G.; Collins, L.; Merikanto, J.; Minikin, A.; Hamburger, T.; Jean-Philippe, P.; Carsten, G.; et al. Primary versus secondary contributions to particle number concentrations in the European boundary layer. *Atmos. Chem. Phys.* **2011**, *11*, 12007–12036. [[CrossRef](#)]
117. Lovejoy, E.R. Atmospheric ion-induced nucleation of sulfuric acid and water. *J. Geophys. Res.* **2004**, *109*, D08204. [[CrossRef](#)]
118. Kawamura, K.; Kasukabe, H.; Barrie, L.A. Secondary formation of water-soluble organic acids and α -dicarbonyls and their contributions to total carbon and water-soluble organic carbon: Photochemical aging of organic aerosols in the Arctic spring. *J. Geophys. Res. Atmos.* **2010**, *115*, D21306. [[CrossRef](#)]
119. Yttri, K.E.; Lund Myhre, C.; Eckhardt, S.; Fiebig, M.; Dye, C.; Hirdman, D.; Strom, J.; Klimont, Z.; Stohl, A. Quantifying black carbon from biomass burning by means of levoglucosan—A one-year time series at the Arctic observatory Zeppelin. *Atmos. Chem. Phys.* **2014**. [[CrossRef](#)]
120. Moroni, B.; Cappelletti, D.; Ferrero, L.; Crocchianti, S.; Busetto, M.; Mazzola, M.; Becagli, S.; Traversi, R.; Udisti, R. Local vs. long-range sources of aerosol particles upon Ny-Ålesund (Svalbard Islands): Mineral chemistry and geochemical records. *Rend. Lincei* **2016**, *27*, S115–S127. [[CrossRef](#)]
121. Castro-Jiménez, J.; Berrojalbiz, N.; Wollgast, J.; Dachs, J. Polycyclic aromatic hydrocarbons (PAHs) in the Mediterranean Sea: Atmospheric occurrence, deposition and decoupling with settling fluxes in the water column. *Environ. Pollut.* **2012**, *166*, 40–47. [[CrossRef](#)] [[PubMed](#)]
122. Hung, H.; Blancharda, T.P.; Halsall, C.J.; Bidlemanc, T.F.; Sternd, G.A.; Felling, P.; Muir, D.C.G.; Barrieg, L.A.; Jantunena, L.M.; Helmd, P.A.; et al. Temporal and spatial variabilities of atmospheric polychlorinated biphenyls (PCBs), organochlorine (OC) pesticides and polycyclic aromatic hydrocarbons (PAHs) in the Canadian Arctic: Results from a decade of monitoring. *Sci. Tot. Environ.* **2005**, *342*, 119–144. [[CrossRef](#)] [[PubMed](#)]
123. Aas, W.; Breivik, K. *Heavy Metals and POP Measurements*; EMEP/CCC-Report 4/2013; NO-2027; Norwegian Institute for Air Research: Kjeller, Norway, 2011.
124. Fu, P.Q.; Kawamura, K.; Chen, J.; Charriere, B.; Sempère, R. Organic molecular composition of marine aerosols over the Arctic Ocean in summer: Contributions of primary emission and secondary aerosol formation. *Biogeosciences* **2013**, *10*, 653–667. [[CrossRef](#)]
125. Cecinato, A.; Mabilia, R.; Marino, F. Relevant organic components in ambient particulate matter collected at Svalbard Islands (Norway). *Atmos. Environ.* **2000**, *34*, 5061–5066. [[CrossRef](#)]
126. Pietrogrande, M.C.; Mercuriali, M.; Perrone, M.G.; Ferrero, L.; Sangiorgi, G.M.L.; Bolzacchini, E. Distribution of n-Alkanes in the Northern Italy Aerosols: Data Handling of GC-MS Signals for Homologous Series Characterization. *Environ. Sci. Technol.* **2010**, *44*, 4232–4240. [[CrossRef](#)]
127. Gelpi, E.; Schneider, J.; Mann, J.; Oro, J. Hydrocarbons of geochemical significance in microscopic algae. *Phytochemistry* **1970**, *9*, 603–612. [[CrossRef](#)]
128. Saliot, A. Natural hydrocarbons in sea water. In *Marine Organic Chemistry*; Duursma, E., Dawson, R., Eds.; Elsevier: New York, NY, USA, 1981; pp. 327–374.
129. Eichmann, R.; Neljling, P.; Ketseridis, G.; Hahn, J.; Jaenicke, R.; Junge, C. n-Alkane studies in the troposphere-I: Gas and particulate concentrations in North Atlantic Air. *Atmos. Environ.* **1979**, *13*, 587–599. [[CrossRef](#)]

130. Rudnick, R.L.; Gao, S. *Composition of the Continental Crust, in Treatise on Geochemistry*; Elsevier: Oxford, UK, 2003; pp. 1–64.
131. Giardi, F.; Becagli, S.; Traversi, R.; Frosini, D.; Severi, M.; Caiazzo, L.; Ancillotti, C.; Cappelletti, D.; Moroni, B.; Grotti, M.; et al. Size distribution and ion composition of aerosol collected at Ny-Ålesund in the spring–summer field campaign 2013. *Rend. Lincei* **2016**, *27*, S47–S58. [[CrossRef](#)]
132. Becagli, S.; Anello, F.; Bommarito, C.; Cassola, F.; Calzolari, G.; Di Iorio, T.; di Sarra, A.; Gómez-Amo, J.L.; Lucarelli, F.; Marconi, M.; et al. Constraining the ship contribution to the aerosol of the central Mediterranean. *Atmos. Chem. Phys.* **2017**, *17*, 2067–2084. [[CrossRef](#)]



© 2019 by the authors. Licensee MDPI, Basel, Switzerland. This article is an open access article distributed under the terms and conditions of the Creative Commons Attribution (CC BY) license (<http://creativecommons.org/licenses/by/4.0/>).